Foreland magmatism during the Arabia – Eurasia collision: Pliocene-Quaternary activity of the Karacadağ Volcanic Complex, SW Turkey

Taner Ekici[1*], Colin G. Macpherson[2], Nazmi Otlu[1], Denis Fontignie[3]

[1] Department of Geological Engineering, University of Cumhuriyet, 58140, Sivas, Turkey

[2] Department of Earth Sciences, University of Durham, Durham, DH1 3LE, UK.

3 Department of Mineralogy, University of Geneva, CH-1205 Geneva, Switzerland.

* Corresponding author:
tanere7@gmail.com
Tel: +903462191010/1928
Fax: +902191171

Running Title: Quaternary Petrogenesis of Mt. Karacadağ

Submitted draft for *Journal of Petrology*
13 May 2014

ABSTRACT

Pliocene to Quaternary magmatism in the Karacadağ Volcanic Complex in southeast Turkey occurred in the foreland region of the Arabia - Eurasia collision and can be divided into two phases. The earlier Karacadağ phase formed a north-south trending volcanic ridge that erupted three groups of lavas. The same range of mantle sources contributed to the younger Ovabağ phase lavas which were erupted from monogenetic cones to the east of the Karacadağ fissure. Like several other intraplate localities across the northern Arabian Plate this magmatism represents mixtures of melt from shallow, isotopically enriched mantle and from deeper, more depleted mantle. The deep source is similar to the depleted mantle invoked for other northern Arabian intraplate volcanic fields but at Karacadağ this source contained phlogopite. This source could be located in the shallow convecting mantle or may represent a metasomatic layer in the base of the lithosphere. There is no evidence for a contribution from the Afar mantle plume, as has been proposed elsewhere in northern Arabia. Melting during the Karacadağ and Ovabağ phases could have resulted from a combination of upwelling beneath weak or thinned lithosphere and restricted local extension of that weakened lithosphere as it collided with Eurasia. Tension associated with the collision focussed magma of the Karacadağ phase into the elongate shield volcano of Mt. Karacadağ. The northern end of the fissure accommodated more extensive differentiation of magma, with isolated cases of crustal contamination, consistent with greater stress in the lithosphere closest to the collision. Most magma batches of the Karacadağ and Ovabağ phases differentiated by fractional crystallisation at ~ 5 MPa, near the boundary between the upper and lower crust. Magma batches dominated by melt from garnet lherzolite show evidence for restricted amounts of differentiation at ~ 22.5 MPa, which is close to the base of the lithospheric mantle.

Keywords: Arabia; fissure volcano; intraplate; Karacadağ; Turkey.

INTRODUCTION

The Arabian Plate hosts several basaltic volcanic fields and so provides a valuable natural laboratory to explore intraplate magmatism (Camp and Roobol 1992; Ilani et al., 2001; Shaw et al., 2003; Krienitz et al., 2006, 2007 and 2009; Ma et al., 2011). Intraplate magmatism occurred in clusters from 30 to 16 Ma and/or from 13 to 8 Ma in southern Turkey (e.g. Gaziantep, Kilis, Karacadağ; Gürsoy et al., 2009; Lustrino et al., 2010 and 2012; Ekici et al., 2012), in northern Syria (Krienitz et al., 2006), in the Syrian Dead Sea Fault (Ma et al., 2011) and in the Harrat Ash Shaam (Shaw et al., 2003; Krienitz et al., 2007), with a significant increase in activity since the Pliocene (Ilani et al., 2001). Most of this activity occurred close to and parallel to, although not always within, tectonic structures such as the Dead Sea Fault Zone, Euphrates Graben, Sirhan Graben, Karak Graben and Esdraelon Valley (Fig. 1a). Some of these structures, for example the Euphrates Graben, experienced no tectonic activity during magmatism.

The Karacadağ Volcanic Complex in southeast Turkey (Fig. 1), sometimes referred to as Karacalıdağ, is one of a number of such fields distributed along the northern edge of the Arabian Plate, where it has collided with Anatolia (Allen et al., 2004). Until recently, magmatism from this complex was reported to be very young (Pearce et al., 1990; Şen et al., 2004). New geochronological data for the Siverek plateau lavas, which constitute the earliest activity of the complex, indicate that activity began no later than the Middle Miocene (Lustrino et al., 2010 and 2012; Ekici et al., 2012). Petrogenetic models for the Karacadağ Volcanic Complex, and for other intraplate fields in northernmost Arabia, have tended to concentrate on the proximity of the Arabian – Anatolian collision in seeking a geodynamic context for magmatism (e.g. Keskin, 2003; Krientiz et al., 2006). The recognition of multiple phases of magmatism demonstrates that the Karacadağ Volcanic Complex is not the result of a single event or process. In a previous publication we discussed the petrogenesis of

the Miocene Siverek plateau lavas (Ekici et al., 2012). In this contribution we turn our attention to the younger magmatism. Lustrino et al. (2012) have shown this is geochemically distinct from the earlier Siverek phase. Our analysis reveals further levels of distinction within each of the two young phases of activity at the complex. We explore the genesis and differentiation of this magmatism in the context of tectonic activity associated with the developing collision and the structure of the Arabian Plate.

GEOLOGICAL SETTING

The Karacadağ Volcanic Complex, in southeast Turkey, lies immediately south of the Arabian – Anatolian Collision Zone (Fig. 1). The collision is the result of northward motion of the Arabian Plate, with respect to Eurasia and the Anatolian Plate (Allen et al., 2004). During the Paleocene this caused Neo-Tethyan oceanic lithosphere to be subducted beneath Anatolia. Subduction continued until formation of the Bitlis Suture between Arabia and Anatolia (Fig. 1a). Continued convergence between Arabia and Eurasia led to westward extrusion of Anatolia along the Northern- and Eastern Anatolian faults during the Late Miocene (Robertson, 2000; Şengör et al., 2008).

The structure of the northernmost Arabian Plate is relatively poorly known, with most constraints coming from studies in Saudi Arabia, Jordan and Syria. Heat flow measurements and xenolith petrology have been used to estimate that the lithosphere – asthenosphere transition occurs at approximately 80 km depth (McGuire and Bohannon, 1989; Nasir and Safarjalani, 2000; Shaw et al., 2007). Seismic data suggest that beneath 35 km depth a mafic, lower crust is succeeded by a 5 to 8 km-thick mantle transition zone (El-Isa et al., 1987a, b). Both petrologic and seismic evidence indicate that a boundary between upper and lower crust lies close to 19 km beneath the surface (El-Isa et al., 1987b; Nasir, 1992).

The Karacadağ Volcanic Complex has been active since the Middle Miocene when the Siverek phase plateau basalts were produced (Ercan et al., 1990; Lustrino et al.,

2010; Ekici et al., 2012) but is particularly well known for its Late Miocene to Quaternary products (Pearce et al., 1990; Ercan et al., 1990; Adıyaman and Chorowicz, 2002; Keskin, 2003; Şen et al., 2004; Brigland et al., 2007; Demir et al., 2007; Lustrino et al., 2010). This younger activity can be grouped into two further phases, termed Karacadağ and Ovabağ.

During the Late Miocene to Quaternary alkali basaltic and basanitic lavas were erupted from Mt. Karacadağ, a north-south fissure volcano approximately 25 km in length. We refer to three summits on the volcanic axis as the northern, central and southern summits (Fig. 1b). Individual lavas from Mt Karacadağ initially flowed east or west, extending up to 15 km to either side of the volcanic ridge. The lava fields also extend up to 25 km north and south of the fissure. Nine Ar-Ar measurements yield ages ranging from 4.50 to 0.91 Ma (Ekici et al., submitted), which agree with prior radiometric measurements for Mt. Karacadağ (Pearce et al., 1990; Lustrino et al., 2010). Adıyaman and Chorowicz (2002) have suggested that the northern end of Mt. Karacadağ lies at the southern end of a WNW-ESE fault extending from the East Anatolian Fault. The Karacadağ fissure indicates that the lithosphere was under tensional stress during this stage of the collision, although there is little evidence that this part of the northern margin of the Arabian Plate experienced significant east-west extension.

Products of the youngest phase of activity in the complex lie approximately 15 km to the east of Mt. Karacadağ, around the village of Ovabağ (Fig. 1b). These are predominantly alkali basalt flows erupted from monogenetic cones and cover approximately 150 km^2. The youngest of these flows, erupted from the 100m high Baruttepe cone, is exceptionally fresh although there is little evidence of alteration of any of the Ovabağ flows. Most of these were erupted from cones, similar to Baruttepe, and flowed east up to 20 km from the eastern flank of Mt. Karacadağ before being channelled into river valleys and flowing up to a further 5 km east or southeast. The flows are vesicular and often retain flow structures such as pahoehoe

surfaces and surface break-out structures. Vesicles are generally empty and only rarely contain secondary calcite. Similar monogenetic cones occur further to the east and south of the Karacadağ Volcanic Complex, towards the border with Syria. Ekici et al. (submitted) obtained an Ar-Ar ages of 0.29Ma ± 0.13 and 0.53Ma (± 1.14) for an Ovabağ lava, which is consistent with the geomorphological evidence of very recent activity.

ANALYTICAL METHODS

Seventy-six fresh samples, forty-eight from Mt. Karacadağ and twenty-eight from Ovabağ, were analysed for major and trace element concentrations at ACME laboratories (Canada; Table 1). Any calcite-bearing vesicles were avoided when preparing material for analysis. Major element analyses were conducted by X-ray fluorescence upon fused discs prepared by using six parts of lithium tetraborate and one part of rock powder. The mixture was fused in crucibles of 95% Pt and 5% Au at 1050°C for 60 minutes to form a homogeneous melt that was cast into a thick glass disc. Trace element concentrations were analysed by ICP-MS using a fusion method. Precision was monitored using an internal standard (SO-18) while accuracy was calibrated using standards W-2, GSP-2, BCR-2, SY4 and SY-3 (Supplementary Tables 1 & 2). Uncertainty on these measurements is better than ± 3 % for major element oxides and ± 10 % for trace elements.

Isotope ratios of Pb, Sr, and Nd were measured on splits separated from the same 0.2 g aliquots at the University of Geneva using a 7-collector Finnigan MAT 262 thermal ionisation mass spectrometer during December 2008. Samples were processed using procedures described in Chiaradia et al. (2011). The 90° magnetic sector mass analyser has an extended geometry with stigmatic focusing. $^{87}Sr/^{86}Sr$ and $^{143}Nd/^{144}Nd$ ratios were measured in semi-dynamic mode, using double Re filaments. Conventional Pb isotope ratio measurements were obtained in dynamic mode with a single Re filament. $^{88}Sr/^{86}Sr = 8.375209$ was used to correct the mass

fractionation of $^{87}Sr/^{86}Sr$, which was compared to the NIST-SRM987 $^{87}Sr/^{86}Sr$ value of 0.710240 ($^{87}Sr/^{86}Sr_{measured}$ = 0.710240 ± 0.000012 (2 σ), n = 31). $^{143}Nd/^{144}Nd$ was mass fractionation corrected relative to a $^{146}Nd/^{144}Nd$ value of 0.721903 and normalized to the Nd La Jolla standard value of 0.511835 ($^{143}Nd/^{144}Nd_{measured}$ = 0.511845 ± 0.000004 (2 σ), n = 26). Lead isotope data were corrected for instrumental mass fractionation and machine bias by applying a discrimination factor determined by multiple analyses of NBS SRM981, using the reference value of Todt et al. (1984). The discrimination factor averaged 0.00082 +/- 0.00005 (2 SE, n = 132) per mass unit. External reproducibility (2 σ) of the standard ratios are 0.05% for $^{206}Pb/^{204}Pb$, 0.08% for $^{207}Pb/^{204}Pb$ and 0.10% for $^{208}Pb/^{204}Pb$. These standard analyses were performed during a 6-month period in which the Karacadağ lavas were analysed. Pb, Sr and Nd blanks were all below their respective detection limits.

RESULTS

Petrography

All lavas from Mt. Karacadağ itself are alkaline, being alkali basalts, trachybasalts, basanites and tephrites, with rare phonotephrite. Most lavas are very fresh, the vast majority having low Loss on Ignition (LOI) values of less than 1 % (Table 1). The lavas are fine grained and porphyritic, containing olivine and plagioclase phenocrysts, up to 25 modal %, set in a matrix of the same minerals, plus clinopyroxene, which is occasionally titanium-rich and oxides. Phenocrysts are generally 0.2 – 1 mm in size with groundmass crystals less than 0.1 mm. Plagioclase phenocrysts show some signs of disequilibrium with sieve textures observed in a number of samples. Such disequilibrium might arise from magma-mixing or contamination (Dungan and Rhodes, 1978) but could also result from decompression or heating (Nelson and Montana 1992; Thy et al., 2013). Therefore, the sieve textures, in themselves, do not provide evidence for open system behaviour.

Lavas from Ovabağ are exceptionally fresh as shown by their very low, and frequently positive, LOI, which is due to iron oxidation during ignition. These lavas include basalts, alkali basalts, trachybasalts and rare tephrites. Like Karacadağ phase lavas these are fine-grained flows but differ in the predominance of olivine phenocrysts. Again, there is a range of phenocryst contents, up to 25 modal %. Titanaugite is more common than at Karacadağ, sometimes as micro-phenocrysts, but usually as part of the groundmass.

Results

Lavas from both phases can be split into three groups based on geochemistry. In the discussion below these are referred to as groups K1, K2 and K3 for the Karacadağ Phase and O1, O2 and O3 for the Ovabağ phase. Similarities between Karacadağ groups and Ovabağ groups will be mentioned where appropriate.

Karacadağ Phase

Lavas from both the Karacadağ and Ovabağ phases show similar ranges of major and trace element compositions to those observed by prior studies (Fig. 2 and 3). Karacadağ phase lavas display a much wider range in compositions than those from Ovabağ. Group K1 lavas have lower MgO (2.2 – 6.7 wt. %) and higher Al_2O_3 (> 15 wt. %) than the remaining two Karacadağ groups (Fig. 2). In groups K2 and K3 MgO is generally greater than 8 wt. % but K3 is offset to lower SiO_2 and Al_2O_3 and to higher TiO_2, Fe_2O_3, Na_2O, K_2O and P_2O_5 for any particular MgO content. Most major element oxides correlate well with MgO, particularly in group K1, although Fe_2O_3 and TiO_2 display more scatter than others due to an inflection at around 5 wt. % MgO. The major element groupings of the Karacadağ phase are also readily apparent in trace element concentrations. Nickel contents of K2 and K3 lavas are similar to one another and significantly greater than those of K1 (Table 1). Within each group of the Karacadağ phase concentrations of incompatible elements increase with decreasing MgO (Fig. 3).

In mantle normalised plots all Karacadağ phase lavas show patterns that are enriched in the most incompatible elements, peaking at Nb, and depleted in the heavy rare earth elements and Y (Fig. 4). A striking negative Pb anomaly is apparent in the patterns of all groups. Patterns for K1 and K2 lavas are very similar but with greater concentrations in the former, consistent with their lower MgO contents. Group K3 lavas have more elevated concentrations of incompatible elements than those from group K2 (Fig. 2) but with similar shaped patterns (Fig. 4b and c), except for the presence of negative K anomalies in most K3 samples. The magnitude of this anomaly is not linked to MgO content but it is more pronounced in silica-poor rocks (Fig. 5a and b).

Group K3 lavas display the lowest values of $^{87}Sr/^{86}Sr$ and $\Delta 7/4$ and $\Delta 8/4$, and the highest values of $^{143}Nd/^{144}Nd$ (Table 2 and Fig. 6) of any lava from the Karacadağ Volcanic Complex. Ratios for the other two Karacadağ groups largely overlap one another but a K1 sample (DK-58) displays the most radiogenic Sr and least radiogenic Nd isotopic ratios in this study. However, these values are not as extreme as noted for the Miocene Siverek plateau lavas (Fig. 6). With the exception of DK-58, the ranges of isotopic ratios are similar to those previously observed for intra-plate magmatism elsewhere in the northern Arabian Plate (Shaw et al., 2003; Krienitz et al., 2009; Ma et al., 2011).

Ovabağ Phase

All Ovabağ lavas contain more than 8 wt. % MgO. Group O1 lavas have higher SiO_2 and Al_2O_3, and lower CaO, Fe_2O_3, TiO_2, K_2O and Na_2O than O3 lavas at similar MgO. The restricted ranges in composition make it difficult to resolve systematic variations of other major elements with MgO within each group. Group O2 lavas are relatively scarce in our dataset and have the highest SiO_2 and lowest K_2O, TiO_2, Na_2O for any MgO content in the Ovabağ phase (Fig. 2). Groups O1 and O3 display parallel, negative correlations between MgO and Ni (not shown), while O3 lavas are

consistently enriched in incompatible elements compared to O1 at a particular MgO content (Fig. 3). Group O2 lavas have the lowest incompatible element contents of the Ovabağ groups.

Comparing the Ovabağ and Karacadağ phases with one another, concentrations of major and incompatible trace elements in Group O1 lavas most closely resemble Group K2 but possess slightly higher SiO_2 and K_2O (and most incompatible trace elements), and lower Fe_2O_3 and TiO_2 (Fig. 2 and 3). Several O1 lavas also show minor, positive K anomalies (Fig. 5b). The shapes of O2 lavas in the multi-element plot are similar to O1 but, as noted above, have lower concentrations of all incompatible elements (Fig. 4). The greatest distinction of group O3 from other Ovabağ lavas is their negative K anomalies, which are not as pronounced as seen in group K3 but are, again, associated with lower silica contents (Fig. 5b). Lavas from groups K3 and O3 are very similar with respect to many major and trace elements (Fig. 2 and 3) and trace element ratios (Fig. 4 and 5).

Lavas from the Ovabağ Phase of magmatism display more restricted ranges of radiogenic isotope ratios than the Karacadağ Phase (Table 2). The lowest $^{87}Sr/^{86}Sr$ and highest $^{143}Nd/^{144}Nd$ ratios occur in group O3, with values approaching those of group K3 (Fig. 6). A lava from group O1 (DO-68) possesses Sr, Nd and Pb isotopic ratios that lie within the range of the K1 and K2 lavas. The remaining Ovabağ lavas have isotopic ratios that lie within the range previously observed for other northern Arabian intraplate volcanic fields (Fig. 6).

DISCUSSION

The existence of multiple magmatic phases within the Karacadağ Volcanic Complex has only been reported recently (Lustrino et al., 2010; Ekici et al., 2012). Previously, the complex, along with its sources and causative mechanisms, was regarded as having a short magmatic history (e.g. Pearce et al. 1990; Keskin, 2003). Lustrino et al. (2012) recognised differences between the major and trace element geochemistry

of Karacadağ and Ovabağ phase lavas and attributed this to a long term secular change in source compositions that included the preceding Siverek plateau lavas. The range in $^{87}Sr/^{86}Sr$ that we have recognised is similar to that documented by Lustrino et al. (2012) but offset to slightly lower values. Our new data reveal a significantly larger range in $^{143}Nd/^{144}Nd$, largely due to the small number of samples for which Lustrino et al. (2012) determined Nd isotopic ratios.

We have previously documented that much of the isotopic variation of the Siverek lavas can be attributed to crustal contamination (Ekici et al., 2012). Our new data reveal that there are significant variations in major and trace element chemistry within both the Karacadağ and Ovabağ phases. For Mt. Karacadağ this variation also involves a spatial aspect, with K1 lavas being clustered close to the northern summit and K3 close to the central summit (Fig. 1b). Thus, before evaluating changes in the mantle sources we must determine the role of differentiation, including crustal contamination, in generating the chemical diversity of the Karacadağ and Ovabağ lavas.

Fractional Crystallisation

Most lavas in this study possess relatively high MgO contents. The main exception to this is group K1 in which MgO varies between 2.3 and 6.7 wt. %, suggesting moderate to extensive differentiation of primary magma. Some K3 lavas also show slightly more evolved compositions with MgO contents of c. 6 wt. %. To examine whether fractional crystallisation could generate the variations within these groups we undertook modelling using alphaMELTS software (Smith and Asimow, 2005).

The low MgO contents of K1 lavas suggest that none of these represent a parental magma but most ratios of incompatible trace element in K1 lavas are very similar to those of group K2 (Figs. 4 and 5). Therefore, we selected a primitive group K2 lava, KD-102, as the starting composition with which to attempt to replicate variations within group K1. For K3 lavas, which cannot be produced from a K2 parent, we

chose KD-26, the member of this group with the most elevated MgO. Relatively low water contents (0.35 wt. %) were required for both parent compositions and the oxygen fugacity was set at the QFM buffer. More extreme values for either of these parameters failed to generate suitable models. Specifically, elevated fO_2 resulted in early oxide saturation while more elevated H_2O supressed plagioclase crystallisation in lower pressure models. An iterative approach revealed that only a narrow range of differentiation conditions replicated the compositional variation of each group.

Major element variations of group K1 can be replicated through fractional crystallisation of KD-102 at 5 MPa. In this model the initial stages of crystallisation, which account for removal of less than 10 % of the original mass of melt, are dominated by olivine with minor spinel. This stage is able to generate much of the major element variation observed in the K2 group, although there is some scatter of the alkali and alkaline earth metals (see below). Group K1 closely resemble melts generated after olivine is replaced on the liquidus by clinopyroxene at c. 7 wt. % MgO (Fig. 7). The proportion of spinel crystallising in the 5 MPa model increases significantly at 5 wt. % MgO, which corresponds to a significant inflection in TiO_2, Fe_2O_3 and V in the K1 array (Fig. 3 and 7) although some groundmass clinopyroxene in K1 lavas is titanaugite, which could also contribute to depletion of these elements. At around 4 wt. % MgO the model precipitated plagioclase. This is consistent with the very minor inflections for Al_2O_3 (Fig. 2 and 7) at which point slightly less than 40% of the original melt had crystallised. The models are also consistent with petrographic observations of olivine ± clinopyroxene ± oxide ± plagioclase phenocryst assemblages in most Karacadağ phase lavas.

To explore the role of fractional crystallisation further we examined the ratios of incompatible trace elements with similar bulk partition coefficients. Most group K1 and K2 lavas show no systematic variation in such ratios with changing MgO (Fig. 5). There is relatively little variation of these ratios and almost complete overlap in the ratios of groups K1 and K2 (Fig. 5). Therefore, we are confident that the model

329 generated from the alphaMELTS software captures the important features of
330 differentiation in these groups. However, there are two deviations from expected
331 behaviour. First, Sm/Zr shows a systematic change within group K1 (Fig. 5f). This
332 appears to be part of a progressive depletion in the middle (M-) and heavy rare earth
333 elements (HREE), relative to other elements with similar compatibility, with
334 decreasing MgO in K1 lavas. Since the absolute concentrations of REEs increase
335 with decreasing MgO (c.f. ytterbium in Fig. 2) we attribute this to the MREE and
336 HREE behaving slightly less incompatibility than normally expected during
337 crystallisation of the magma. Second, a small subset of group K1 has elevated K/La
338 and Ba/Yb at a particular value of MgO. Because Ba/Yb has previously been
339 proposed as a proxy for crustal contamination in the Karacadağ Volcanic Complex
340 we have identified this subset as Group K1a in Figures 3, 5 and 7. Their
341 development is discussed in the next section.

342 Group K3 compositions cannot be generated from a K2 parent, or vice versa.
343 Therefore, the K3 series records a distinct initial melt, while its major element
344 variations suggest differentiation under different conditions. In particular, garnet
345 crystallisation is required to suppress Al_2O_3 enrichment (with decreasing MgO) whilst
346 matching the other K3 major element characteristics. For the DK-26 parent
347 composition the optimum alphaMELTS model involves differentiation at 22.5 MPa,
348 initially of 5 % orthopyroxene with minor spinel followed by removal of an
349 assemblage comprising garnet, clinopyroxene and spinel. This achieves the
350 enrichment of K_2O and N_2O whilst suppressing Al_2O_3 and SiO_2 enrichment and also
351 depleting CaO in the melt (Fig. 7).

352 Ovabağ Phase lavas display restricted ranges in concentrations of all major
353 elements implying that fractional crystallisation played a limited role in the evolution
354 of these melts. Like group K2, the restricted variations within groups O1 and O2 can
355 be replicated by removal of less than 10% olivine, with minor spinel, from a parental

356 basalt with around 10 wt. % MgO. The similarity of group O3 to group K3 suggests
357 that these also differentiated at relatively high pressure.

358 **Crustal contamination**

359 Crustal contamination is known to have affected Neogene and Quaternary
360 magmatism throughout the Arabian Plate (Baker et al., 2000; Shaw et al., 2003;
361 Krienitz et al., 2009; Ma et al., 2011). For example, despite the absence of crustal
362 xenoliths or xenocrysts in the Miocene Siverek magmatism of the Karacadağ
363 Volcanic Complex, variations towards higher $^{87}Sr/^{86}Sr$, $\Delta 7/4$ and $\Delta 8/4$ and lower
364 $^{143}Nd/^{144}Nd$ demonstrate that some of those lavas interacted with the crust (Ekici et
365 al., 2012). Contamination was not a ubiquitous process, however, with only some
366 Siverek lavas displaying an isotopic signature of interaction with the crust. This
367 contamination had a negligible impact on incompatible trace element contents and
368 ratios, except for enriching Ba with respect to other elements. Selective Ba
369 enrichment most probably occurred because the contamination leverage for this
370 element – its concentration in the contaminant relative to the magma - was
371 significantly higher than that of other elements.

372 Concentrations of incompatible trace elements in Pliocene – Quaternary lavas are
373 similar to or greater than those in the most trace element enriched Siverek basalts.
374 Therefore, the same set of country rocks should exert even less contamination
375 leverage upon incompatible trace element concentrations in Karacadağ and Ovabağ
376 phase magma than was the case for Siverek. This is evaluated further in Fig. 5.
377 Rocks containing more than 8 wt. % MgO display the full range for most of the
378 incompatible trace element ratios and show no obvious correlations either within
379 particular groups or in the datasets as a whole. This observation suggests that
380 ranges for these ratios were present in the most primitive magma batches and that
381 crustal contamination had a negligible impact upon the trace element chemistry of
382 Mg-rich magma. The highest Ba/Yb ratios occur in the two most evolved members of

group K3 (Fig. 5). Yet, these same two samples show the lowest $^{87}Sr/^{86}Sr$, $\Delta 7/4$ and $\Delta 8/4$, and highest $^{143}Nd/^{144}Nd$ observed for the Karacadağ and Ovabağ phases, suggesting that a crustal influence was not required to generate the range of trace element ratios observed in this magmatism.

Further insight comes from comparing the incompatible trace element ratios of groups K1 and K2, which were shown to be related by fractional crystallisation (previous section). The small subset of K1a lavas, with elevated Ba/Yb and K/La at a given value of MgO, include sample DK-58 (Fig. 5), which possesses the most extreme isotopic characteristics of all the Pliocene – Quaternary lavas (Fig. 6). However, the changes to incompatible trace element ratios are small and not systematic for all elements. For example, while group K1a lavas all have elevated K/La and Ba/Yb (Fig. 5c), some do not show elevated K_2O or Ba at a given MgO content, relative to the rest of group K1 (Fig. 3). Similarly, there are some other group K1 lavas that have elevated K_2O and Ba but not elevated K/La and Ba/Yb. There are negligible differences of the concentrations of most major and trace elements in groups K1 and K1a. Only the alkali and alkaline earth elements show systematic, although small, enrichments in the latter (Figs. 3 and 7). These, apparently contradictory, observations probably reflect the low contamination leverage of most crustal rocks on the trace element contents of magma from the Karacadağ Volcanic Complex. Thus, while the K1a group suggests some magma – crust interaction occurred, the restricted magnitude of variations suggest that most trace element and isotopic ratios in Karacadağ and Ovabağ phase magma were not modified significantly by crustal contamination.

Modelling the contamination that has occurred is hampered by the absence of data for suitable crustal rocks for northern Arabia, a problem which has been recognised by several studies (Shaw et al., 2003; Krienitz et al., 2006 and 2009; Ma et al., 2011). To estimate the amount of melt – crust interaction we employed the approach of Ekici et al. (2012) who used Sudanese lithologies to investigate crustal

411 contamination of Siverek plateau basalts. These offer a range of Sr, Nd and Pb
412 isotopic compositions with which to constrain the role of crustal rocks. In taking this
413 approach we are not trying to advocate any shared provenance between Sudanese
414 and Turkish basement but are testing the suitability of upper versus lower crustal
415 rocks as contaminants within the northern Arabian lithosphere. Since the K2 group
416 are parental to group K1 we used the K2 sample with the most elevated $^{143}Nd/^{144}Nd$
417 (KD-29) as the primitive magma in these models.

418 Contamination of a magma with the initial isotopic composition of DK-29 by lower
419 crust provides a good fit to Sr and Nd ratios of DK-58 with only a restricted amount of
420 differentiation (F = 0.93) for a relatively high ratio of assimilation to crystallisation (r =
421 0.75; model LC in Fig. 6). Contamination by upper crust does not produce such low
422 $^{143}Nd/^{144}Nd$ relative to $^{87}Sr/^{86}Sr$ as seen in DK-58. The lower crust model also
423 provides a more suitable fit to the displacement of DK-58 in Pb isotope space.
424 However, the amount of contaminant required to produce the Sr and Nd isotopic
425 variation would, in most cases, lead to substantially more extreme Pb isotopic ratios
426 than observed in DK-58. This may be because the parental melt was significantly
427 richer in Pb than DK-29 or the crust beneath Karacadağ was able to exert
428 considerably less Pb isotopic leverage than these models suggest. In either case,
429 the amount of contamination suggested by Pb is substantially less than estimated
430 from $^{87}Sr/^{86}Sr$ and $^{143}Nd/^{144}Nd$ for DK-58. Therefore, the Sr and Nd isotope data
431 provide an upper limit for contamination of 5% and suggests most batches of magma
432 experienced substantially less contamination than this.

433 **Composition of mantle sources**

434 Crustal contamination introduced little isotopic and trace element heterogeneity into
435 magma of the Karacadağ and Ovabağ phases. Therefore, most of the variation in
436 these lavas must have existed in their parental magmas. Previous studies of
437 northern Arabian Plate volcanism have advocated peridotitic sources with elemental

438 concentrations resembling primitive mantle (Shaw et al., 2003; Ekici et al., 2012). In
439 addition, Ma et al. (2011) invoked garnet-bearing hornblendite veins to explain the
440 incompatible trace element characteristics of low-silica lavas from the northern Dead
441 Sea Fault. In this section, we shall explore the origin of the variation in the source of
442 Karacadağ Volcanic Complex lavas. Since group K1 experienced greater
443 differentiation than the remaining groups we shall exclude these whilst constraining
444 the trace element characteristics of sources beneath the north Arabian Plate.
445 However, we shall include relevant K1 data when using isotopic ratios to place
446 further constraints upon those sources.

447 Ovabağ data show how the rare earth element systematics of the Karacadağ
448 Volcanic Complex lavas can be reconciled with fractional, non-modal melting of
449 peridotite with element concentrations resembling primitive mantle, with or without a
450 small amount of MREE enrichment (Shaw et al., 2003; Ekici et al., 2012). Groups O2
451 through O1 to O3 form a shallow, positive array in Dy/Yb versus La/Yb space (Fig.
452 8a). The low Dy/Yb ratios in the group O2 lavas coincide with the spinel lherzolite
453 melting model suggesting low degrees of melting (2 to 3 %) of a relatively shallow
454 source. Groups O1 and O3 form a tight cluster trending from O2 values towards a
455 restricted range of compositions with high Dy/Yb and La/Yb, which would represent
456 low degree (< 1.5 %) partial melting of a garnet lherzolite. Therefore, groups O2 and
457 O3 represent mixtures of melt from primitive spinel lherzolite with progressively
458 greater amounts of melt derived from below the spinel - garnet transition. The tight
459 array suggests little variation in the degree of partial melting in the shallow and deep
460 sources. The greater prominence of low degrees of partial melting implied for the
461 group O3 lavas is also consistent with their higher trace element contents (Fig. 3).
462 Groups K2 and K3 can be interpreted in a similar way but are displaced from the
463 Ovabağ array to intersect the modelled melting curves at higher degrees of melting
464 (Fig. 8a). In addition, the more elevated Dy/Yb values in group K3 also indicate a
465 greater relative contribution from garnet lherzolite.

Models invoking primitive mantle concentrations of REEs provide valuable information on the relative contributions from different depths during polybaric melting of the mantle. But Karacadağ Volcanic Complex lavas show fractionation of large ion lithophile elements from both the rare earth elements and high field strength elements, which cannot be produced by melts of primitive spinel- and garnet-lherzolite alone (Fig. 8c). These fractionations also preclude an origin involving only a primitive mantle and hornblendite veins as proposed by Ma et al. (2011), which cannot generate the $(K/La)_n$ values greater than one that are common to groups K2, O1 and O2. The low K/La and K/Nb ratios of group K3 lavas could be interpreted as reflecting derivation from a source containing hornblendite (Fig. 8c) but their elevated and variable Dy/Yb ratios are not consistent with this origin (Fig. 8a). Furthermore, low Sm/Zr ratios suggest a limited or non-existent role for this lithology in the genesis of all Karacadağ Volcanic Complex lavas (Fig. 8d).

Incompatible trace element ratios of Karacadağ and Ovabağ lavas are not consistent with derivation from a carbonated mantle (Nelson et al., 1988; Blundy and Dalton, 2000; Dixon et al., 2008; Sisson et al., 2009). They display low Ba/Th and elevated Nb/La, with the most silica-poor (Mg-rich) liquids possessing the lowest La/Nb (Fig. 5e), and Zr depletion is negligible (Fig. 4 and Fig. 5f). These signatures also contrast with those proposed for carbonated mantle in the northern Arabian Plate (Shaw et al., 2007). Therefore, in an attempt to reproduce the incompatible trace element variation we modelled melting of hydrous garnet lherzolite (Fig. 9). Fractional, non-modal melting was modelled for two sources. First, we explored the amphibole-bearing source and melting proportions given by Ma et al. (2011). The second model was a phlogopite-garnet peridotite of Sisson et al. (2009) using partition coefficients from Sisson et al. (2009) and Adam and Green (2011). Neither model, by itself, reproduces the range of compositions observed in the Karacadağ Volcanic Complex lavas or in the different groups that we have identified. However, mixtures of melts from phlogopite-bearing mantle and anhydrous sources with a small enrichment of

494 the most incompatible elements can achieve many of the key characteristics (Sisson
495 et al., 2009).

496 Mixtures between melt from an amphibole-garnet lherzolite and anhydrous, enriched
497 (garnet- or spinel-) lherzolite cannot reproduce the low Ba/La and Ba/Yb and
498 relatively high Zr/Nb ratios seen in many of the lavas from the Karacadağ and
499 Ovabağ phases (Fig. 9a, c and d). This source does, however, provide a particularly
500 good fit to Jordanian Harrat Ash Shaam lavas (Shaw et al., 2007) for all ratios except
501 Rb/Ba (see below). This suggests that the trace element enrichment of magmatism
502 close to the Syrian – Jordanian border may be due to the presence of significant
503 amounts of amphibole in the mantle (Fig. 9a, c and d) but amphibole does not
504 appear be an important component in the mantle beneath Karacadağ.

505 Although melts from phlogopite-garnet lherzolite are not suitable as sole sources
506 they do display some of the key trace element features that characterise the
507 Karacadağ and Ovabağ lavas. Elevated Zr/Nb at low K/La, and low Ba/Yb and Ba/La
508 are all predicted for melts derived from this source (Fig. 9a,c and d). Since REE
509 systematics suggest derivation over a range of depths (Fig. 8a) we suggest that the
510 Pliocene to Quaternary Karacadağ Volcanic Complex lavas were derived from
511 mixtures of melt derived from three sources: phlogopite-bearing garnet lherzolite,
512 enriched garnet lherzolite and enriched spinel lherzolite. No simple binary mixtures
513 can reproduce the entire data array. However, mixtures of 1.5 to 5 % partial melts of
514 phlogopite-garnet-peridotite with low degree (< 1 %) partial melts from anhydrous
515 lherzolite reproduce most of the key features (Fig. 9a,c and d). The major problem
516 comes in reproducing the low Rb/Ba ratios of the northern Arabian intra-plate
517 magmatic suites (Fig. 9). We have tried various manipulations of the models to
518 achieve low Rb/Ba, particularly coupled to elevated La/Yb (Fig. 9b) whilst
519 maintaining the fits achieved for other ratios. We speculate that the most likely
520 solution is a relatively high partition coefficient for Rb in phlogopite (e.g. $D_{Rb}^{phlog} > 8$),
521 which is not unreasonable (Ionov et al., 1997).

Thus, we propose that most Karacadağ Volcanic Complex lavas originated as mixtures of (i) melt derived from enriched, anhydrous lherzolite over a range of depths, with (ii) melt derived from phlogopite-bearing garnet lherzolite. While lavas from Harrat Ash Shaam or the northern Dead Sea Fault appear to record evidence for amphibole in their sources (Shaw et al., 2003; Ma et al., 2011) there is little evidence to support its involvement at Karacadağ (Figs. 8 and 9). Having invoked three-component mixing in the mantle, it is difficult to also place more quantitative constraints on the degree of partial melting. However, using the REEs, which should be modified by metasomatism in a relatively systematic fashion, suggests that the Pliocene to Quaternary Karacadağ Volcanic Complex lavas formed through small degrees of partial melting similar to those calculated for other parts of the northern Arabian Plate (Fig. 7a).

Origin of mantle sources

Prior studies have identified a number of potential mantle sources beneath the Arabian Plate that could contribute to intraplate magmatism. These include lithospheric mantle, variably enriched by metasomatism or metasomatic phases, the convecting upper mantle and outflow of mantle derived from the Afar triple junction (Çapan et al., 1987; Pearce et al., 1990; Camp and Roobol, 1992; Bertrand et al., 2003; Shaw et al., 2003; Şen et al., 2004; Weinstein et al., 2006; Krienitz et al., 2006, 2007 and 2009; Lustrino et al., 2010; Ma et al., 2011; Ekici et al., 2012). Most of these studies have identified multiple components at any one site. In this section we shall evaluate the isotopic ratios of Pliocene to Quaternary magmatism in the Karacadağ Volcanic Complex relative to other locations in the northern Arabian Plate and the implications for mantle sources throughout this area.

Karacadağ Volcanic Complex lavas lack $^{206}Pb/^{204}Pb$ in excess of 19.1, in contrast to the Harrat Ash Shaam, Dead Sea Fault and northern Syria, where a high $^{206}Pb/^{204}Pb$ component has been invoked (Bertrand et al., 2003; Krienitz et al., 2009; Ma et al.,

549 2011). This component is most conspicuous in high-$^{206}Pb/^{204}Pb$ lavas from Karasu
550 Valley and Dead Sea Fault from which a $^{206}Pb/^{204}Pb$ ratio greater than 19.5, with
551 $^{207}Pb/^{204}Pb$ and $^{208}Pb/^{204}Pb$ ratios close to the Northern Hemisphere Reference Line,
552 can be inferred (Fig. 6c and d). This high-$^{206}Pb/^{204}Pb$ component was attributed to
553 the Afar plume by Krienitz et al. (2009) although others have suggested it was an
554 older, lithospheric source (Bertrand et al., 2003). A clear distinction between the $\Delta 8/4$
555 values of Afar plume magmatism and Arabian intraplate lavas, including the
556 Karacadağ Volcanic Complex, precludes involvement of Afar plume in magmatism of
557 the northernmost Arabian Plate (Fig. 6d). Regardless of its origin, however, the high-
558 $^{206}Pb/^{204}Pb$ component has not made a significant contribution to Karacadağ
559 Volcanic Complex magmatism.

560 A group K3 lava displays the lowest $^{207}Pb/^{204}Pb$ and $^{208}Pb/^{204}Pb$ for a given
561 $^{206}Pb/^{204}Pb$ of any sample from the Karacadağ Volcanic Complex. The Sr and Nd
562 isotopic ratios of this sample (DK-25) are similar to low-$^{206}Pb/^{204}Pb$ samples from
563 Harrat Ash Shaam and northern Syria (Bertrand et al., 2003; Shaw et al., 2003;
564 Krienitz et al., 2009). Therefore, we interpret this as an endmember that is common
565 to much of the intraplate magmatism across northern Arabia and, as previously
566 suggested by Shaw et al. (2003) and Krienitz et al. (2009), the low $^{206}Pb/^{204}Pb$, $\Delta 7/4$,
567 $\Delta 8/4$ and $^{87}Sr/^{86}Sr$ and high $^{143}Nd/^{144}Nd$ indicate that this is probably depleted upper
568 mantle. Rare earth element systematics demonstrate that group K3 lavas contain a
569 relatively large contribution from the garnet stability field and so the distinctive K3
570 isotopic composition could reflect melt derived from either lithospheric or
571 asthenospheric mantle. Workman and Hart (2005) characterised the long-known
572 range of compositions in the depleted mantle as a spectrum spanning enriched (E-
573 DMM) to depleted (D-DMM) end-members. The isotopic ratios of DK-25 are very
574 similar to those of E-DMM, which is likely to represent the most fusible component of
575 the convecting mantle. Therefore, the K3 composition might represent small degree
576 melts from the convecting mantle, in which phlogopite can be stable (Luth, 2003).

577 Alternatively, such melts may metasomatise the base of the lithospheric mantle
578 (McKenzie, 1989) providing a hydrated lherzolite source resembling E-DMM that
579 could contribute to magmatism generated throughout the region. Kovács et al.
580 (2012) suggest that phlogopite would be the primary hydrous phase in peridotite at
581 pressures greater than 3 GPa although the presence of this and alternative water-
582 bearing phases at lower pressures, principally the amphibole pargasite, is also
583 dependent on the bulk composition and the absolute water content of the mantle.

584 Incompatible element systematics indicate that group K1 and K2 lavas contain
585 greater contributions from shallower mantle (Fig. 8 and 9). Melting at shallow levels
586 could occur if asthenosphere upwells sufficiently to melt to higher degrees, so
587 allowing increased dilution of the E-DMM component by melts from more refractory
588 parts of the mantle (Elliott et al., 1991). However, this is not consistent with the
589 higher $^{87}Sr/^{86}Sr$ and lower $^{143}Nd/^{144}Nd$ of the group K1 and K2 lavas (Fig. 6). In
590 addition, large degrees of asthenospheric upwelling would be difficult to reconcile
591 with limited or highly localised extensional tectonics during magmatism at Mt.
592 Karacadağ (Adiyaman and Chorowicz, 2002). Therefore, we suggest that the lavas
593 of groups K1 and K2 are dominated by melts derived from enriched parts of the
594 shallow lithospheric mantle. The enriched, lithospheric source possesses $^{87}Sr/^{86}Sr$ ~
595 0.70370 and $^{143}Nd/^{144}Nd$ ~ 0.51286. Pb isotope ratios are more difficult to constrain
596 due to the possible influence of crustal contamination. However, the enriched
597 lithosphere is likely to have slightly lower $^{206}Pb/^{204}Pb$ than the depleted component
598 and slightly more elevated $\Delta 7/4$ and $\Delta 8/4$ (Fig. 6).

599 Shaw et al. (2003) concluded that the Jordanian part of the Harrat Ash Shaam was
600 also derived from mixtures of deep, depleted and shallow, enriched mantle. Despite
601 the evidence for differences in the nature of hydrous phases between Karacadağ
602 and Harrat Ash Shaam (Fig. 9), the isotopic data indicate that the two volcanic
603 regions are probably derived from similar types of mantle.

Magma transport through the crust at Mt. Karacadağ

The thickness of individual lava flows was not measured as part of this study so we cannot quantify the relative volumes of magma generated by different parts of the Karacadağ volcano. However, most lavas initially flowed laterally from the loci of eruption therefore some constraints can be obtained by observing where each group predominates along the ridge crest. We combine this information with constraints obtained from fractional crystallisation models to interpret magma transport during the Karacadağ Phase of magmatism. Group K1 lavas were mainly erupted on and around the northern summit of Mt. Karacadağ but were much less abundant on the central and southern summits (Fig. 1b). Lavas of group K2, in contrast, are present along the length of the ridge. This suggests that the magmatic plumbing at the northern end of the volcano was conducive to eruption of magma that had differentiated more extensively.

Late Cenozoic stress in the northern Arabian Plate was produced by its collision with Anatolia. The resultant westward escape of Anatolia, accommodated in southern Turkey along the East Anatolian Fault (Fig. 1a), has caused different types of strain throughout northern Arabia. Adıyaman and Chorowicz (2002) attributed the Mt Karacadağ fissure to far-field, east – west tension that diminished towards the south, distal to the collision. If this tensional stress diminished southward along the Karacadağ fissure then the northern part of the volcano could have provided a larger accommodation volume in the crust into which more magma could be emplaced. This, in turn, would supply more heat into surrounding crustal rocks, which would account for the northern K1 group providing the few examples where we observed evidence for crustal contamination. A differentiation pressure of 5 MPa, as determined for groups K1 and K2 from the alphaMELTS models, indicates crystallisation close to the postulated upper to lower crust transition of 19 km (Nasir and Safarjalani, 2000). This depth has also been proposed as the transition from brittle to ductile behaviour of crust in northern Arabia (Adıyaman and Chorowicz,

2002). Thus, we suggest that differentiation could proceed further at the northern end of Mt. Karacadağ as a result of relatively large volumes of magma ponding close to the petrological and rheological boundary between upper and lower crust (Fig. 10). Elsewhere along the fissure, the cooler crust would have impeded development of extensive storage zones and magma experienced less differentiation, resulting in the more primitive K2 lava flows.

Group K3 has a restricted distribution on the Mt. Karacadağ ridge, being the predominant lava type of the central summit with a minor presence on the northern summit (Fig. 1b). Most of these have elevated MgO contents and the fractional crystallisation models reflect very restricted amounts of differentiation. The distinctive chemistry of this group, however, does require differentiation high at pressure (Fig. 7) and it is tempting to equate the modelled pressure of 22.5 MPa with the 80 km depth estimated for the lithosphere – asthenosphere transition zone in northern Arabia (McGuire and Bohannon, 1989; Nasir and Safarjalani, 2000). The lack of evidence for low pressure crystallisation suggests that, subsequent to fractionation close to the base of the lithosphere, group K3 magmas experienced negligible further differentiation before eruption.

CONCLUSIONS

Mt. Karacadağ is the most conspicuous feature of the Karacadağ Volcanic Complex, forming an elongate shield volcano that has produced lateral lava flows from its north – south oriented axis. This form suggests that lithospheric tension localised magmatism during the Pliocene and Quaternary. East-west tension in this part of the Arabian Plate was the result of local stress due to the initiation of the Eastern Anatolian Fault (Adıyaman and Chorowicz, 2002). Late in the history of the Karacadağ Volcanic Complex magmatism migrated to Ovabağ, where lavas were erupted from monogenetic cones and represent melting and emplacement in the absence of significant lithospheric tension.

659 Previously, we interpret the earlier, Miocene phase of magmatism as the result of
660 melting when mantle upwelled beneath a lithospheric weak-spot as the Arabian Plate
661 migrated north and east during the Cenozoic (Ekici et al., 2012). The Karacadağ and
662 Ovabağ phases may represent renewed melting through this process although
663 localised tectonic processes served to focus magmatism. In the case of Mt.
664 Karacadağ, localised extension may also have played a role in causing melting but
665 there is restricted geological evidence at the surface to support this. Isotopic data
666 indicate that mantle derived from the Afar plume was not involved in genesis of
667 Karacadağ Volcanic Complex lavas.

668 Trace element systematics of the Karacadağ Volcanic Complex lavas were
669 influenced by the presence or absence of small quantities (< 2 %) of phlogopite in
670 the mantle. The lavas do not display evidence for derivation exclusively from
671 amphibole veins in the mantle as proposed for magmatism from Al Ghab volcanic
672 field in the Dead Sea Fault (Ma et al., 2011) or for melting of carbonated mantle
673 (Shaw et al., 2007).

674 Trace element and isotopic ratios of groups K3 and O3 lavas are distinct in their low
675 contents of silica and Al_2O_3 and their elevated TiO_2 and incompatible element
676 contents, relative to other groups. Depletion in potassium, relative to other elements
677 of similar compatibilities, coupled with the absence of extreme Ba enrichment
678 indicates that phlogopite was present in the source of these lavas. These groups
679 display trace element ratios which indicate a relatively large contribution from garnet-
680 facies lherzolite. Isotopic characteristics of the lavas resemble the most fusible part
681 of the convecting upper mantle but such a signature could also be transferred to the
682 base of the lithospheric mantle by migration of low degree melts. This component is
683 common to other volcanic fields across northern Arabia. Once generated, K3 and O3
684 magmas experienced minor differentiation near the base of the lithosphere prior to
685 eruption.

686 Groups K2, O1 and O2 represent melting across a range of depths but with a greater
687 contribution from spinel-lherzolite in the lithospheric mantle than in the K3 and O3
688 groups. These groups also have more elevated $^{87}Sr/^{86}Sr$ and Pb isotopic ratios and
689 lower $^{143}Nd/^{144}Nd$ than groups K3 and O3. Group K2 were produced along the length
690 of the 30 km Karacadağ fissure and crystallised limited amounts of olivine close to
691 the transition between upper and lower crust. At the northern end of the Mt.
692 Karacadağ volcano more protracted differentiation of K2 parental magma at the
693 upper – lower crust transition produced magma of group K1. This and the greater
694 amount of crustal contamination observed to the north resulted from greater stress in
695 the crust at the Anatolian end of the Karacadağ fissure. Lavas from groups O1 and
696 O2 show similar trace element and isotopic systematics to Group K2 suggesting that
697 mantle sources sampled by the Karacadağ phase could be generated in the absence
698 of significant lithospheric extension.

699 **ACKNOWLEDGEMENTS**

700 Taner Ekici acknowledges financial support from TUBITAK (Project No. 107Y025) to
701 conduct fieldwork and analytical work. Mehmet Ülkü of MTA Diyarbakır supported
702 fieldwork in SE Turkey. Colin Macpherson is grateful to Durham University for a
703 period of research leave. We thank Mark Allen and Iain Neill for discussion.
704 Comments by Christoph Beier and an anonymous reviewer were very constructive
705 and led to significant improvements in this manuscript, as was the editorial input from
706 Richard Price.

707 **REFERENCES**

708 Adam, J. & Green, T. (2006). Trace element partitioning between mica- and
709 amphibole-bearing garnet lherzolite and anhydrous basanitic melt: 2. Tasmanian
710 Cainozoic basalts and the origins of intraplate basaltic magmas. *Contribution to*
711 *Mineralogy and Petrology* **161**, 883-899, doi:10.1007/s00410-010-0570-7.

712 Adıyaman, Ö. & Chorowicz, J. (2002). Late Cenozoic tectonics and volcanism in the
713 northwestern corner of the Arabian plate: a consequence of the strike-slip Dead Sea
714 fault zone and the lateral escape of Anatolia. *Journal of Volcanology and Geothermal*
715 *Research* **117**, 327-345.

716 Allen, M., Jackson, J. & Walker, R. (2004). Late Cenozoic reorganization of the
717 Arabia-Eurasia collision and the comparison of short-term and long term deformation
718 rates. *Tectonics* **23**, TC2008, doi: 10.1029/2003TC001530.

719 Baker, J.A., Macpherson, C.G., Menzies, M.A., Thirlwall, M.F., Al-Kadasi, M. &
720 Mattey, D.P. (2000). Resolving crustal and mantle contributions to continental flood
721 volcanism, Yemen: Constraints from mineral oxygen isotope data. *Journal of*
722 *Petrology* **41**, 1805-1820.

723 Bertrand, H., Chazot, G., Blichert-Toft, J. & Thoral, S. (2003). Implications of
724 widespread high-μ volcanism on the Arabian Plate for Afar mantle plume and
725 lithosphere composition. *Chemical Geology* **198**, 47-61.

726 Blundy, J. & Dalton, J. (2000). Experimental comparison of trace element partitioning
727 between clinopyroxene and melt in carbonate and silicate systems, and implications
728 for mantle metasomatism. *Contributions to Mineralogy and Petrology* **139**, 356-371.

729 Brigland, D., Demir, T., Seyrek, A., Pringle, M., Westaway, R., Beck, A., Yurtmen, S.
730 & Rowbotham, G. (2007). Dating Quaternary volcanism and incision by the River
731 Tigris at Diyarbakır, SE Turkey. *Journal of Quaternary Science* **21**, 437-455, doi:
732 10.1002/jqs.1074.

733 Camp, V.E. & Roobol, M.J. (1992). Upwelling Asthenosphere beneath western
734 Arabia and its regional implications. *Journal of Geophysical Research* **97**, 15,255-
735 271.

736 Chiaradia, M., Müntener, O. & Beate, B. (2011). Enriched basaltic andesites from
737 mid-crustal fractional crystallization, recharge, and assimilation (Pilavo volcano,
738 Western Cordillera of Ecuador). *Journal of Petrology* **52**, 1107-1141, doi:
739 10.1093/petrology/egr020.

740 Çapan, U.Z., Vidal, P. & Contagrel, L.M. (1987). K-Ar, Nd, Sr and Pb isotopic study
741 of Quaternary volcanism in Karasu Valley (Hatay), N end of Dead Sea rift zone in SE
742 Turkey. *Yerbilimleri* **14**, 165-178.

743 Davidson, J.P. & Wilson, I.R. (1989). Evolution of an alkali basalt-trachyte suite from
744 Jebel Marra volcano, Sudan, through assimilation and fractional crystallisation. *Earth*
745 *and Planetary Science Letters* **95**, 141-160.

746 Demir, T., Westaway, R., Brigland, D., Pringle, M., Yurtmen, S., Beck, A. &
747 Rowbotham, G. (2007). Ar-Ar dating of late Cenozoic basaltic volcanism in northern
748 Syria: Implications for the history of incision by the River Euphrates and uplift of the
749 northern Arabian Platform. *Tectonics* **26**, TC3012, doi:10.1029/2006TC001959.

750 Deniel, C., Vidal, P., Coulon, C., Vellutini, P.J. & Piquet, P. (1994). Temporal
751 evolution of mantle sources during continental rifting: the volcanism of Djibouti (Afar).
752 *Journal of Geophysical Research* **99**, 2853-2869.

753 DePaolo, D.J., 1981. Trace element and isotopic effects of combined wallrock
754 assimilation and fractional crystallisation. *Earth and Planetary Science Letters* **53**,
755 189–202.

756 Dixon, J.E., Clague, D.A., Cousens, B., Monsalve, M.L. & Uhl, J. (2008). Carbonatite
757 and silicate melt metasomatism of the mantle surrounding the Hawaiian plume:
758 evidence from volatiles, trace elements, and radiogenic isotopes. *Geochemistry,*
759 *Geophysics, Geosystems* **9**, Q09005.

760 Dungan, M.A. & Rhodes, M.J. (1978). Residual glasses and melt inclusions in
761 basalts from DSDP legs 45 and 46: evidence for magma mixing. *Contributions to*
762 *Mineralogy and Petrology* **67**, 417-431.

763 Ekici, T., Macpherson, C.G. & Otlu, N. (2012). Polybaric melting of a single mantle
764 source during the Neogene Siverek phase of the Karacadağ Volcanic Complex, SE
765 Turkey. *Lithos* 146-147, 152-163.

766 Ekici, T., Macpherson, C.G. & Otlu, N. (submitted). Intraplate magmatism generated
767 by shear-induced melting during Arabian plate motion: Evidence from Volcanic
768 Complex, southeast Turkey. Submitted to *Journal of the Geological Society of*
769 *London*.

770 Elliott, T.R., Hawkesworth, C.J., & Gronvold, K. (1991). Dynamic melting of the
771 Iceland plume. *Nature* **351**, 201-206.

772 El-Isa, Z., Mechie, J. & Prodehl, C. (1987a). Shear velocity structure of Jordan from
773 explosion seismic data. *Geophysical Journal of the Royal Astronomical Society* **90**,
774 265-281.

775 El-Isa, Z., Mechie, J., Prodehl, C., Makris, J. & Rihm, R. (1987b). A crustal structure
776 study of Jordan derived from seismic refraction data. *Tectonophysics* **138**, 235-253.

777 Ercan, T., Fujitani, T., Matsuda, J.I., Notsu, K., Tokel, S. & ve UI, T. (1990). Doğu ve
778 Güneydoğu Anadolu Neojen-Kuvaterner Volkanitlerine ilişkin yeni jeokimyasal,
779 radyometrik ve izotopik verilerin yorumu. *MTA Dergisi* **110**, 143-164.

780 Gürsoy, H., Tatar, O., Piper, J.D.A., Koçbulut, F. & Mesci, B.L. (2009).
781 Paleomagnetic study of Tertiary volcanic domains in Southern Turkey and Neogene
782 anticlockwise rotation of the Arabian Plate. *Tectonophysics* **465**, 114-127,
783 doi:10.1016/j.tecto.2008.11.001.

784 Hart, S.R. (1984). A large-scale isotope anomaly in the Southern Hemisphere
785 mantle. *Nature* **309**, 753-757.

786 Ilani, S., Harlavan, Y., Tarawneh , K., Rabba, I., Weinberger, R., Ibrahim, K., Peltz,
787 S. & Steinitz, G. (2001). New K-Ar ages of basalts from the Harrat Ash Shaam
788 volcanic field in Jordan: Implications for the span and duration of the upper-mantle
789 upwelling beneath the western Arabian plate. *Geology* **29**, 171-174.

790 Ionov, D.A., Griffin, W.L. & O'Reilly, S.Y. (1997) Volatile-bearing minerals and
791 lithophile elements in the upper mantle. *Chemical Geology* **141**, 153-184.

792 Keskin, M. (2003). Magma generation by slab steepening and breakoff beneath a
793 subduction-accretion complex: An alternative model for collision-related volcanism in
794 Eastern Anatolia, Turkey. *Geophysical Research Letters* **30**, 8046, doi:10,
795 1029/2003GL018019.

796 Krienitz, M.S., Haase, K.M., Mezger, K., Eckardt, V. & Shaikh-Mashail, M.A. (2006).
797 Magma genesis and crustal contamination of continental intraplate lavas in
798 Northwestern Syria. *Contributions to Mineralogy and Petrology* **151**, 698-716,
799 doi10.1007/s00410-006-0088-1.

800 Krienitz, M.S., Haase, K.M., Mezger, K. & Shaikh-Mashail, M.A. (2007). Magma
801 genesis and mantle dynamics at Harrat Ash Shamah volcanic field (Southern Syria).
802 *Journal of Petrology* **48**, 1513-1542, doi:10.1093/petrology/egm028.

803 Krienitz, M.S., Haase, K.M., Mezger, K., Van den Bogard, P., Thiemann, V. &
804 Shaikh-Mashail, M.A. (2009) Tectonics events, continental intraplate volcanism, and
805 mantle plume activity in northern Arabia: Constraints from geochemistry and Ar-Ar
806 dating of Syrian lavas. *Geochemistry Geophysics Geosystems* **10**, Q04008,
807 doi:10.1029/2008GC002254.

808 Kovács, I., Green, D.H., Rosenthal, A., Hermann, J., O'Neil, H.S., Hibberson, W.O. &
809 Udvardi, B. (2012) An experimental study of water in nominally anhydrous minerals
810 in the upper mantle near the water-saturated solidus. *Journal of Petrology* **53**, 2067-
811 2093.

812 Lustrino, M., Keskin, M., Mattioli, M. & Kavan, O. (2012) Heterogeneous mantle
813 sources feeding the volcanic activity of Mt. Karacadağ. *Journal of Asian Earth*
814 *Sciences* **46**, 120-139.

815 Lustrino, M., Keskin, M., Mattioli, M., Lebedev, V.A., Chugaev, A., Sharkov, E. &
816 Kavak, O. (2010). Early activity of the largest Cenozoic shield volcano in the circum-
817 Mediterranean area: Mt. Karacadağ, SE Turkey. *European Journal of Mineralogy* **22**,
818 343-362, doi:10.1127/0935-1221/2010/0022-2024.

819 Luth, R.W. (2003). Mantle volatiles – distribution and consequences, pp. 319-361. In
820 *The Mantle and Core* (ed. R.W. Carlson) Vol 2 *Treatise on Geochemistry* (eds. H.D.
821 Holland & K.K. Turekian), Elsevier-Pergamon, Oxford.

822 Ma, G.S.-K., Malpas, J., Xenophontos, C. & Chan, G.H.-N. (2011). Petrogenesis of
823 latest Miocene-Quaternary continental intraplate volcanism along the northern Dead
824 Sea Fault system (Al Ghab – Homs volcanic field), western Syria: Evidence for
825 lithosphere – asthenosphere interaction. *Journal of Petrology* **52**, 401-430,
826 doi:10.1093/petrology/egq085.

827 McDonough, W.F. & Sun, S.S. (1995). The composition of the Earth. *Chemical*
828 *Geology* **120**, p. 223-253.

829 McGuire, A.V. & Bohannon, R.G. (1989). Timing of mantle upwelling: Evidence for a
830 passive origin for the Red Sea Rift. *Journal of Geophysical Research* **94**, 1677-1682.

831 McKenzie, D. (1989). Some remarks on the movement of small melt fractions in the
832 mantle. *Earth and Planetary Science Letters* **95**, 53-72.

833 Nasir, S. (1992). The lithosphere beneath the northwestern part of the Arabian plate
834 (Jordan): evidence from xenoliths and geophysics. *Tectonophysics* **201**, 357-370.

835 Nasir, S. & Safarjalani, A. (2000). Lithospheric petrology beneath the northern part of
836 the Arabian Plate in Syria: evidence from xenoliths in alkali basalts. *Journal of*
837 *African Earth Sciences* **30**, 149-168.

838 Nelson, S.T. & Montana, A. (1992). Sieve-textured plagioclase in volcanic rocks
839 produced by rapid decompression. *American Mineralogist* **77**, 1242-1249.

840 Nelson, D.R., Chivas, A.R., Chappell, B.W. & McCulloch, M.T. (1988). Geochemical
841 and isotopic systematics in carbonatites and implications for the evolution of ocean-
842 island sources. *Geochimica et Cosmochimica Acta* **52**, 1-17.

843 Pearce, J.A., Bender, J.F., DeLong, S.E., Kidd, W.S.F., Low, P.J., Güner, Y.,
844 Şaroğlu, F., Yılmaz, Y., Moorbath, S. & Mitchell, J.G. (1990). Genesis of collision
845 volcanism in eastern Anatolia, Turkey. *Journal of Volcanology and Geothermal*
846 *Research* **44**, 184-229.

847 Pik, R., Deniel, C., Coulon., Yirgu, G. & Marty, B. (1999). Isotopic and trace element
848 signatures of Ethiopian flood basalts: evidence for plume-lithosphere interactions
849 from Na/Ti and rare earth element ratios. *Journal of Geophysical Research* **104**,
850 2817-2829.

851 Robertson, A.H.F. (2000). Mesozoic-Tertiary tectonic-sedimentary evolution of a
852 south Tethyan oceanic basin and its margins in southern Turkey In: Bozkurt, E.,
853 Winchester, J.A. & Piper, J.D.A. (eds), *Tectonics and Magmatism in Turkey and the*
854 *Surrounding Area. Geological Society of London Special Publications* **173**, 97-138.

855 Şen, P.A., Temel, A. & Gourgaud, A. (2004). Petrogenetic modelling of Quaternary
856 post-collisional volcanism: A case study of central and eastern Anatolia. *Geological*
857 *Magazine* **141**, 81-98, doi: 10.1017/S0016756803008550.

858 Şengör, A.M.C., Özeren, M.S., Keskin, M., Sakınç, M., Özbakır, A.D. & Kayan, İ.
859 (2008). Eastern Turkish high plateau as a small Turkish-type orogen: Implications for
860 post-collisional crust forming processes in Turkish-type orogens. *Earth Science*
861 *Reviews* **90**, 1-48, doi:10.1016/j.earscirev.2008.05.002.

862 Shaw, J.E., Baker, J.A., Menzies, M.A., Thirlwall, M.F. & Ibrahim, K.M. (2003).
863 Petrogenesis of the largest intraplate volcanic field on the Arabian Plate (Jordan): a
864 mixed Lithosphere-Asthenosphere source activated by Lithospheric extension.
865 *Journal of Petrology* **44**, 1657-1679, doi:10.1093/petrology/egg052.

866 Shaw, J.E., Baker, J.A., Kent, A.J.R., Ibrahim, K.M., & Menzies, M.A. (2003). The
867 geochemistry of the Arabian lithospheric mantle – a source for intraplate volcanism?
868 *Journal of Petrology* **48**, 1495-1512.

869 Sisson, T.W., Kimura, J.-I. & Coombs, M.L. (2009). Basanite-nephelinite suite from
870 early Kilauea: carbonated melts of phlogopite-garnet peridotite at Hawaii's leading
871 magmatic edge. *Contributions to Mineralogy and Petrology* **158**, 803-829.
872 doi:10.1007/s00410-009-0411-8.

873 Smith, P.M. & Asimow, P.D. (2005). Adiabat_1ph: A new public front-end to the
874 MELTS, pMELTS, and pHMELTS models. *Geochemistry, Geophysics, Geosystems*
875 **6** Q02004. doi: 10.1029/2004GC000816

876 Thirlwall, M.F., Upton, B.G.J. & Jenkins, C. (1994). Interaction between continental
877 lithosphere and the Iceland plume – Sr-Nd-Pb isotope geochemistry of Tertiary
878 basalts, NE Greenland. *Journal of Petrology* **35**, 839-879.

879 Thy, P., Lesher, C.E. & Tegner, C. (2013). Further work on experimental plagioclase
880 equilibria and the Skaergaard liquidus temperature. *American Mineralogist* **98**, 1360-
881 1367.

882 Todt, W., Cliff, R.A., Hanser, A. & Hoffmann, A.W. (1984). $^{202}Pb+^{205}Pb$ double spike
883 for lead isotopic analyses. *Terra Cognita* **4**, 209.

884 Weinstein, Y., Navon, O., Altherr, R. & Stein, M. (2006). The role of lithospheric
885 mantle heterogeneity in the generation of Plio-Pleistocene alkali basaltic suites from
886 NW Harrat Ash Shaam (Israel). *Journal of Petrology* **47**, 1017-1050.

887 Workman, RK. & Hart, S.R., (2005) Major and trace element composition of the
888 depleted MORB mantle (DMM). *Earth and Planetary Science Letters* **231**, 53-72.

889 **FIGURE CAPTIONS**

890 Figure 1. (a) Location of the Karacadağ Volcanic Complex along with other Neogene
891 to Quaternary volcanic fields at northern margin of Arabian Plate and the locations of
892 major tectonic features in the region. The location of (b) is indicated by a black box.
893 (b) Map of the Karacadağ Volcanic Complex showing the distribution of the
894 Karacadağ and Ovabağ products and sites sampled during this work. Symbols are
895 based on geochemical discrimination (see text for details).

896 Figure 2. Plots of selected major elements versus MgO for Karacadağ and Ovabağ
897 phase lavas from Karacadağ Volcanic Complex. Fields of published data for both
898 phases are from Lustrino et al. (2012) and references therein. Data for Al Ghab and
899 Homs volcanic fields in the northern Dead Sea Fault are from Ma et al. (2011).

900 Figure 3. Plots of selected trace elements versus MgO for Karacadağ and Ovabağ
901 phase lavas from Karacadağ Volcanic Complex. Fields of published data for both
902 phases are from Lustrino et al. (2012) and references therein. Data for Al Ghab and
903 Homs volcanic fields in the northern Dead Sea Fault are from Ma et al. (2011).

904 Figure 4. Ranges of incompatible trace element concentrations in Karacadağ
905 Volcanic Complex lavas normalised to primitive mantle (McDonough and Sun, 1995).
906 Karacadağ phase (a) group K1, (b) group K2 and (c) group K3. Note the more

907 expanded scale in panel (c). Ovabağ Phase (d) group O1, (e) group O2 and (f) group
908 O3.

909 Figure 5. Plots of MgO or SiO_2 versus selected incompatible trace element ratios
910 normalised to primitive mantle (McDonough and Sun, 1995) for Karacadağ and
911 Ovabağ phase lavas from Karacadağ Volcanic Complex.

912 Figure 6. (a) $^{87}Sr/^{86}Sr$ versus $^{143}Nd/^{144}Nd$, (b) $^{206}Pb/^{204}Pb$ versus $^{207}Pb/^{204}Pb$, (c)
913 $^{206}Pb/^{204}Pb$ versus $^{208}Pb/^{204}Pb$, and (d) $\Delta 7/4$ versus $\Delta 8/4$ for Karacadağ and Ovabağ
914 lavas from Karacadağ Volcanic Complex (KVC). Other data from KVC Siverek
915 plateau lavas (Ekici et al., 2012; Lustrino et al., 2010) and from Karasu Valley
916 (Çapan et al., 1987), NW Syria (Krienitz et al., 2006), the Dead Sea Fault in Syria
917 (DSF – Syria; Ma et al., 2011), Harrat Ash Shaam in Jordan (Shaw et al., 2003) and
918 lavas that have been attributed to a plume component beneath Afar (Deniel et al.
919 1994; Pik et al. 1999). Northern Hemisphere Reference Line in (b) and (c) from Hart
920 (1984). Black curves are models of assimilation with fractional crystallisation (De
921 Paolo, 1981) by magma with the composition of lava DK-29. Ticks marks on the
922 curves represent values for melt remaining (F) of 0.999, 0.995, 0.993, 0.99 then 0.01
923 increments to 0.95 and 0.05 increments subsequently. Note than some of these ticks
924 lie beyond the frame of each panel. UC is contamination of DK-29 by upper crust (Sr
925 = 69 ppm, Nd = 18.5 ppm, Pb = 48 ppm, $^{87}Sr/^{86}Sr$ = 0.764478, $^{143}Nd/^{144}Nd$ =
926 0.511398, $^{206}Pb/^{204}Pb$ = 18.598, $^{207}Pb/^{204}Pb$ = 16.026, $^{208}Pb/^{204}Pb$ = 39.746), while
927 LC is contamination by lower crust (Sr = 814 ppm, Nd = 29.94 ppm, Pb = 30 ppm,
928 $^{87}Sr/^{86}Sr$ = 0.709028, $^{143}Nd/^{144}Nd$ = 0.511270, $^{206}Pb/^{204}Pb$ = 16.926, $^{207}Pb/^{204}Pb$ =
929 15.622, $^{208}Pb/^{204}Pb$ = 37.804). Crustal compositions from Davidson and Wilson
930 (1989).

931 Figure 7. Plots of selected major elements versus MgO for Karacadağ phase lavas
932 from Karacadağ Volcanic Complex. Fractional crystallisation models generated using

933 alphaMELTS (Smith and Asimow, 2005) for KD-102 at 5 MPa (solid line) and DK-26
934 at 22.5 MPa (dashed line). See text for more details.

935 Figure 8. (a) La/Yb versus Dy/Yb, (b) Ba/La versus La/Yb, (c) K/Nb versus K/La, and
936 (d) Sm/Zr versus La/Yb for Pliocene to Quaternary Karacadağ Volcanic Complex
937 lavas normalised to primitive mantle (McDonough and Sun, 1995). Data from Al
938 Ghab and Homs in the Dead Sea Fault (Ma et al., 2011) and Harrat Ash Shaam in
939 Jordan (Shaw et al., 2003) included for comparison. Melting models use partition
940 coefficients from Adam and Green (2011), except spinel and potassium in phases
941 not listed in that paper, which use Ma et al. (2011). Melting models for garnet- and
942 spinel-lherzolite use primitive mantle composition of McDonough and Sun (1995),
943 and modal and melting proportions of Thirlwall et al (1994). For hornblendite, the
944 initial composition and melting proportions are from Ma et al. (2011). Tick marks
945 indicate total melt fraction.

946 Figure 9. (a) K/La versus Zr/Nb, (b) La/Yb versus Rb/Ba, (c) La/Yb versus Ba/Yb,
947 and (d) K/Nb versus Ba/La for Pliocene to Quaternary Karacadağ Volcanic Complex
948 lavas normalised to primitive mantle (McDonough and Sun, 1995). For sources of
949 comparator data see caption to Fig. 6. Melting models use abundances of primitive
950 mantle. Garnet-lherzolite (Gt-LH) and spinel-lherzolite (Sp-LH) models are as
951 described in caption to Figure 6, except that large ion lithophile elements were
952 increased by a factor of two (Sisson et al., 2009). Modal and melting proportions are
953 from Ma et al (2011) for amphibole-garnet lherzolite (AG-LH) and from Sisson et al.
954 (2009) for phlogopite-garnet lherzolite (PG-LH). Tick marks indicate total melt
955 fractions.

956 Figure 10. Sketch of petrogenesis at Mt Karacadağ. Siverek plateau basalts were
957 erupted during the Miocene and are the substrate onto which the Karacadağ volcano
958 was erupted. The scale of the vertical axis is schematic and is not intended to be
959 regarded as linear. Constraints on the depth of the upper – lower crust boundary

come from geophysics and xenolith petrology (see text for details). Differentiation depths are from alphaMELTS models. Group K1 and K2 lavas share similar sources that represent polybaric melting but with a relatively large contribution from the spinel stability field, while group K3 lavas contain a larger contribution from deeper, garnet-bearing mantle. Group K2 lavas have experienced relatively restricted amounts of differentiation close to the upper – lower crust boundary and are found along the length of the volcano. Lavas of group K1 occur predominantly in the north and developed when group K2 magma experienced more extensive differentiation at the upper – lower crustal transition. Group K3 lavas experienced small amounts of differentiation close to the base of the lithosphere.

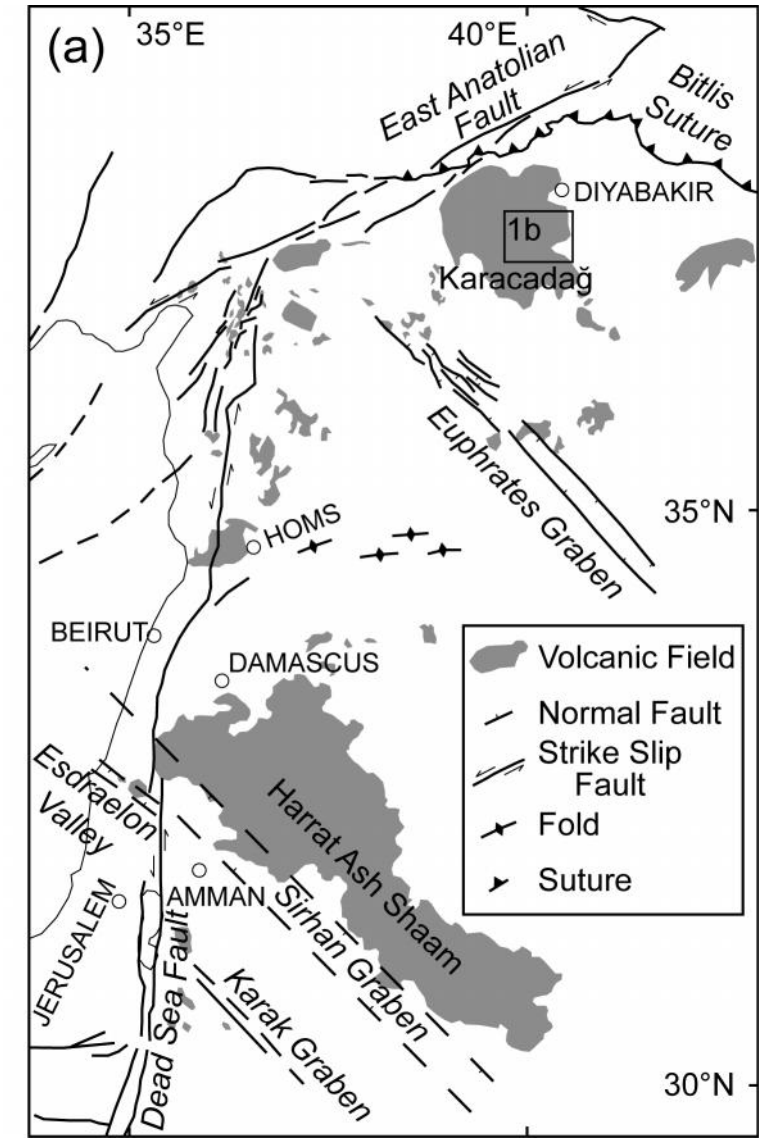

Karacadağ 1a

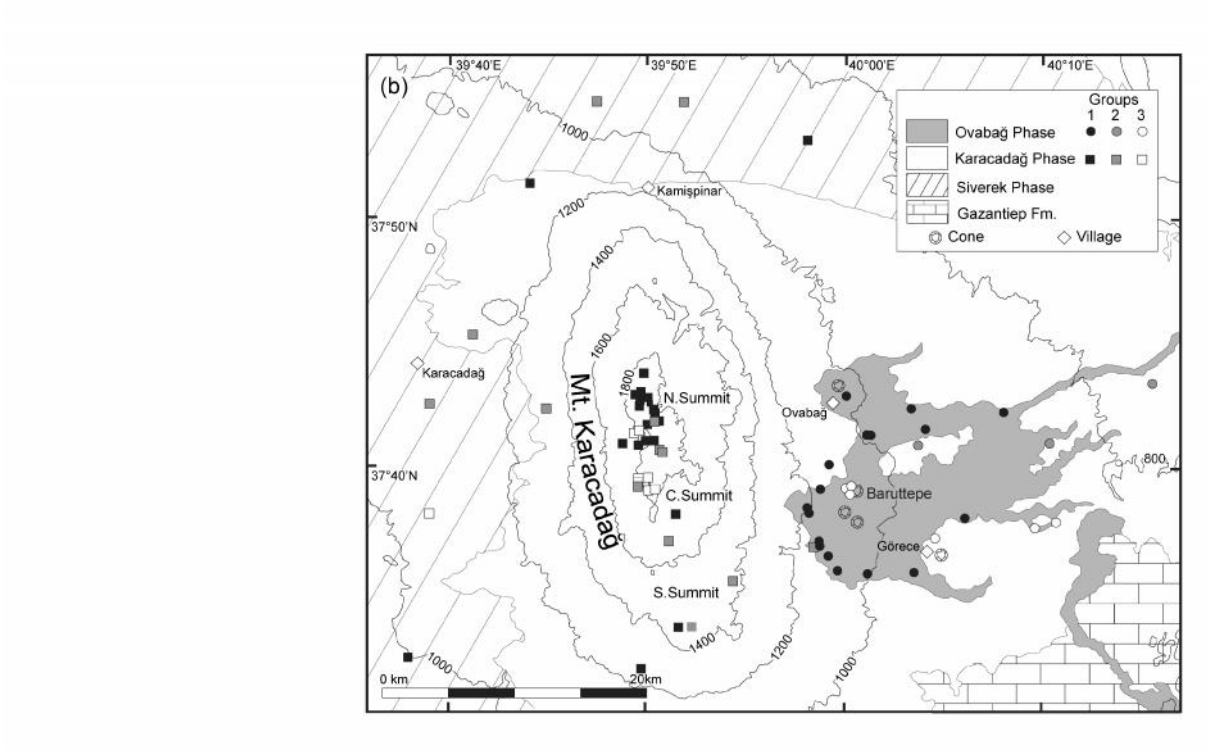

Karacadağ 1b

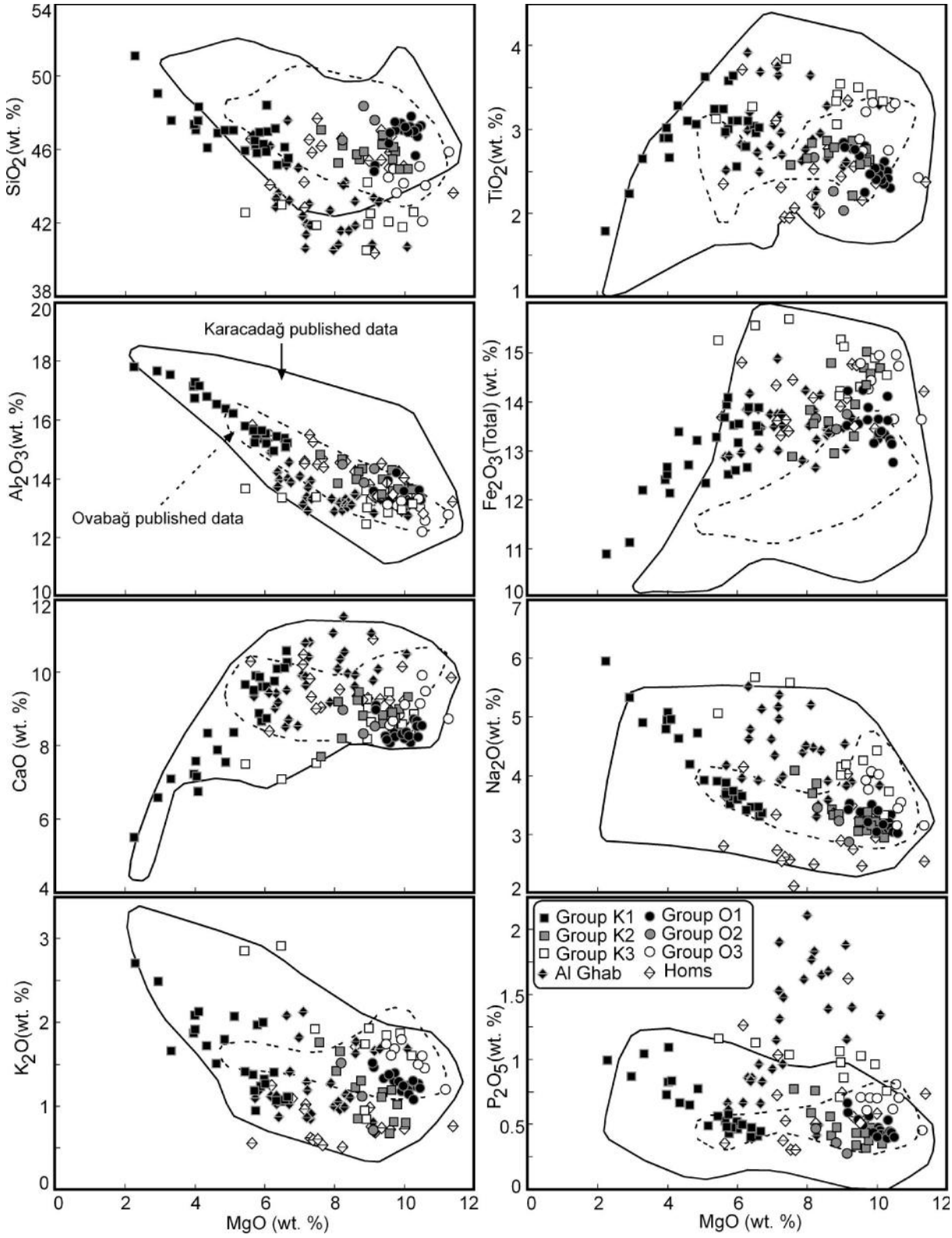
SiO2(wt. %)
TiO2(wt. %)
Al2O3(wt. %)
Karacadağ published data
Ovabağ published data
Fe2O3(Total) (wt. %)
CaO (wt. %)
Na2O(wt. %)
K2O(wt. %)
P2O5(wt. %)
Group K1
Group K2
Group K3
Al Ghab
Group O1
Group O2
Group O3
Homs
MgO (wt. %)
MgO (wt. %)

Karacadağ 2

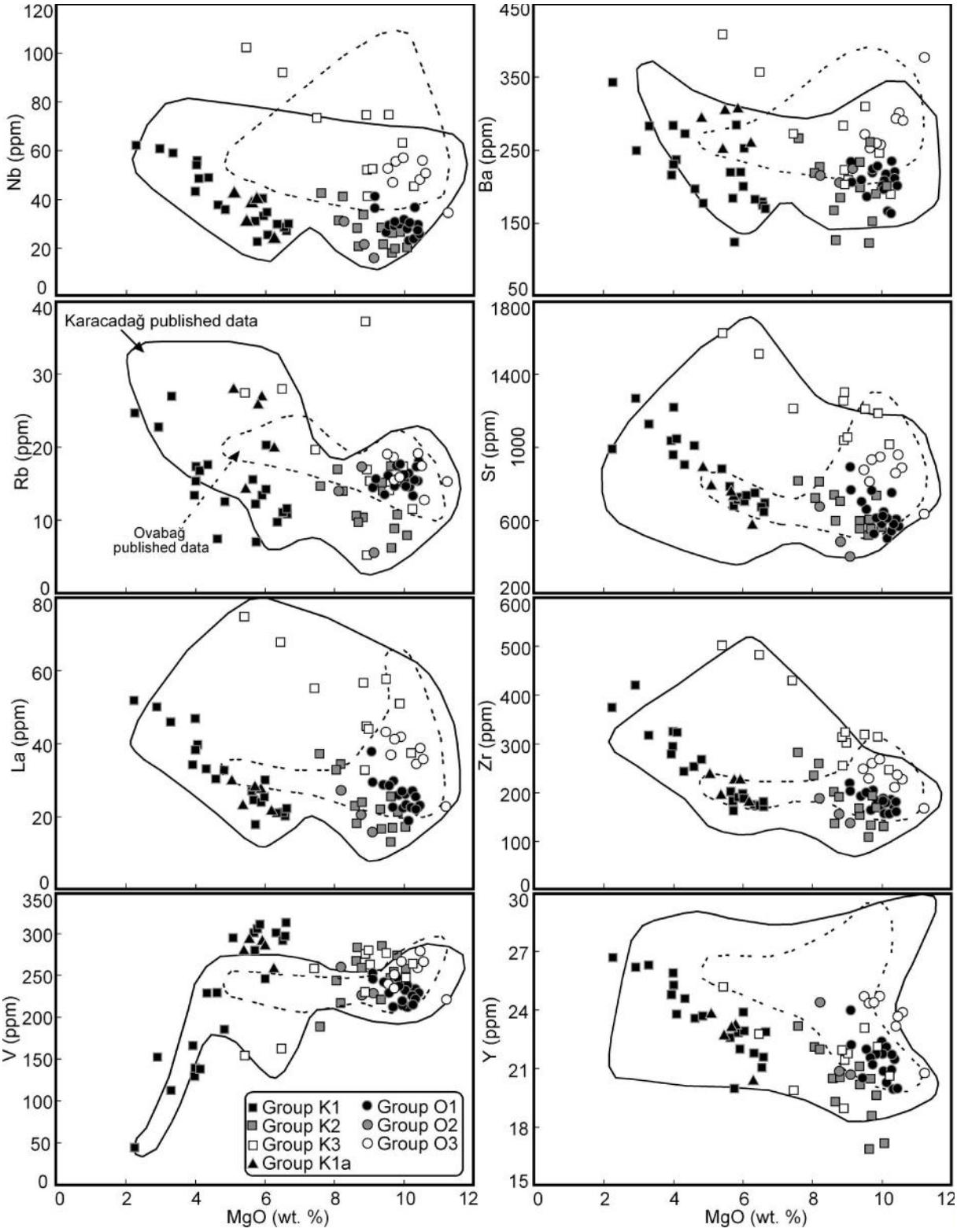
Nb (ppm)
Ba (ppm)
Rb (ppm)
Karacadağ published data
Ovabağ published data
Sr (ppm)
La (ppm)
Zr (ppm)
V (ppm)
Y (ppm)
MgO (wt. %)
MgO (wt. %)
Group K1
Group K2
Group K3
Group K1a
Group O1
Group O2
Group O3

Karacadağ 3

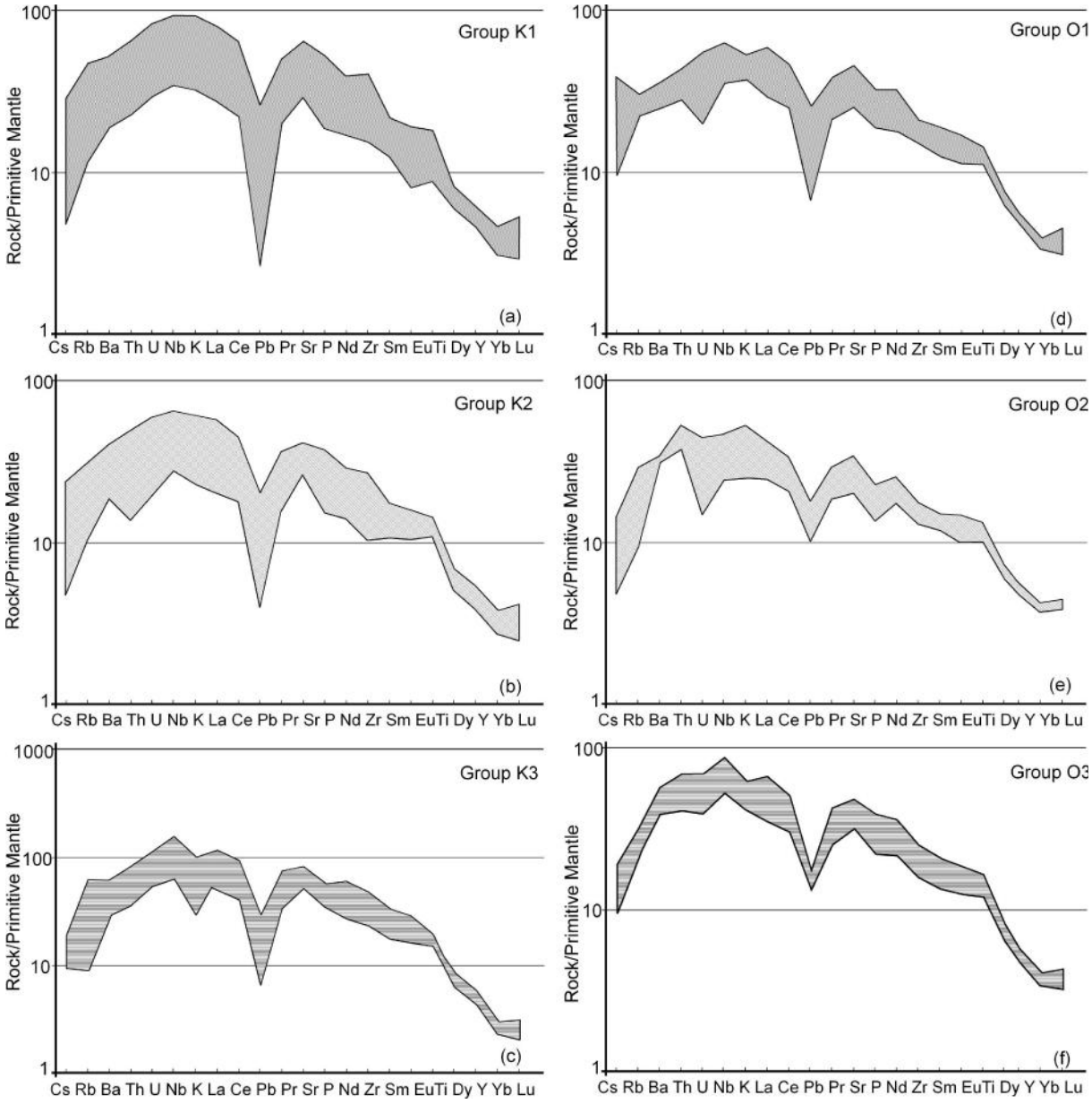
Group K1
Group O1
Group K2
Group O2
Group K3
Group O3
Rock/Primitive Mantle
100
10
1
1000
(a)
(b)
(c)
(d)
(e)
(f)
Cs Rb Ba Th U Nb K La Ce Pb Pr Sr P Nd Zr Sm EuTi Dy Y Yb Lu

Karacadağ 4

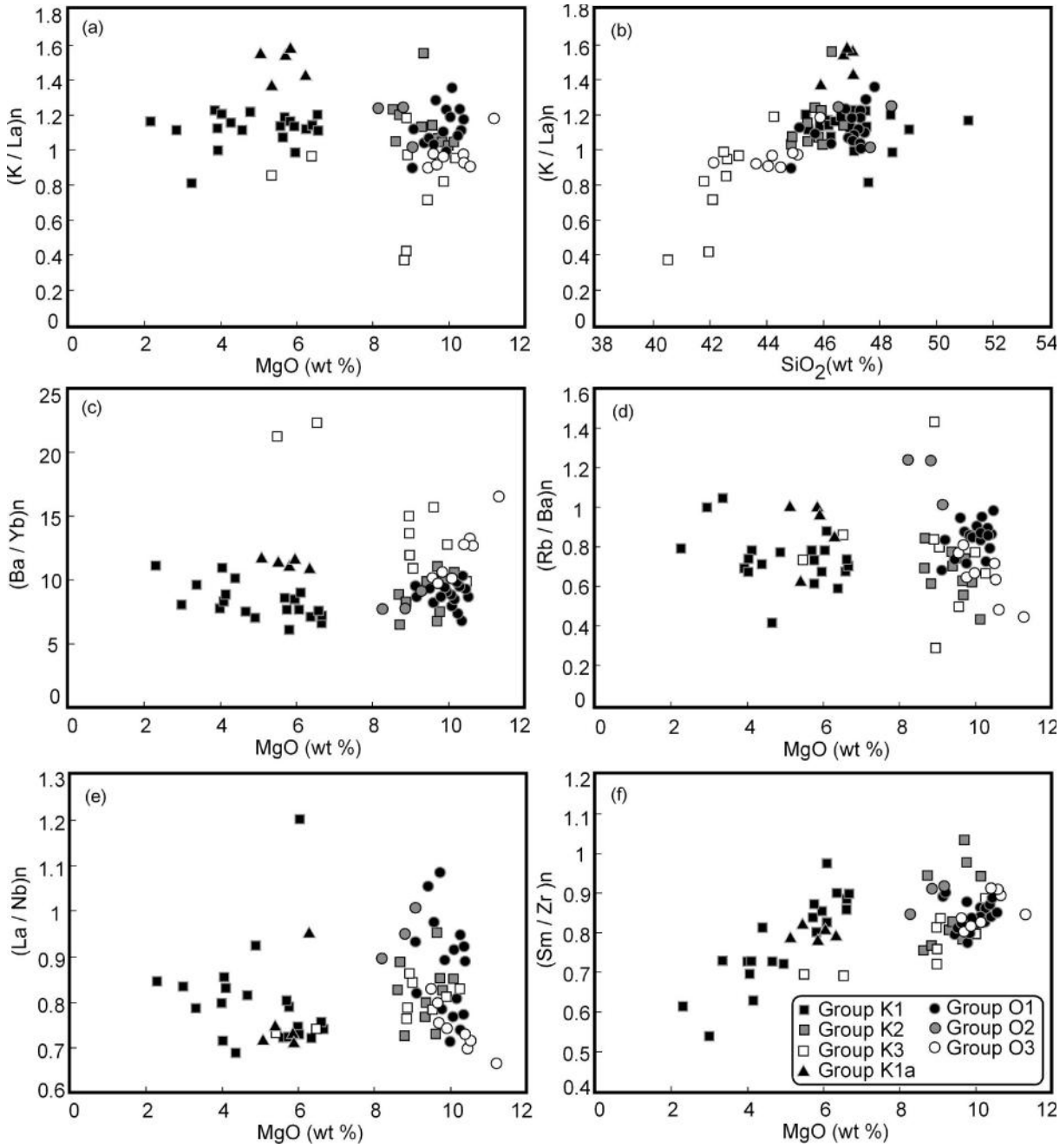
(a)
(K / La)n
MgO (wt %)
(b)
(K / La)n
SiO2(wt %)
(c)
(Ba / Yb)n
MgO (wt %)
(d)
(Rb / Ba)n
MgO (wt %)
(e)
(La / Nb)n
MgO (wt %)
(f)
(Sm / Zr)n
MgO (wt %)
Group K1
Group K2
Group K3
Group K1a
Group O1
Group O2
Group O3

Karacadağ 5

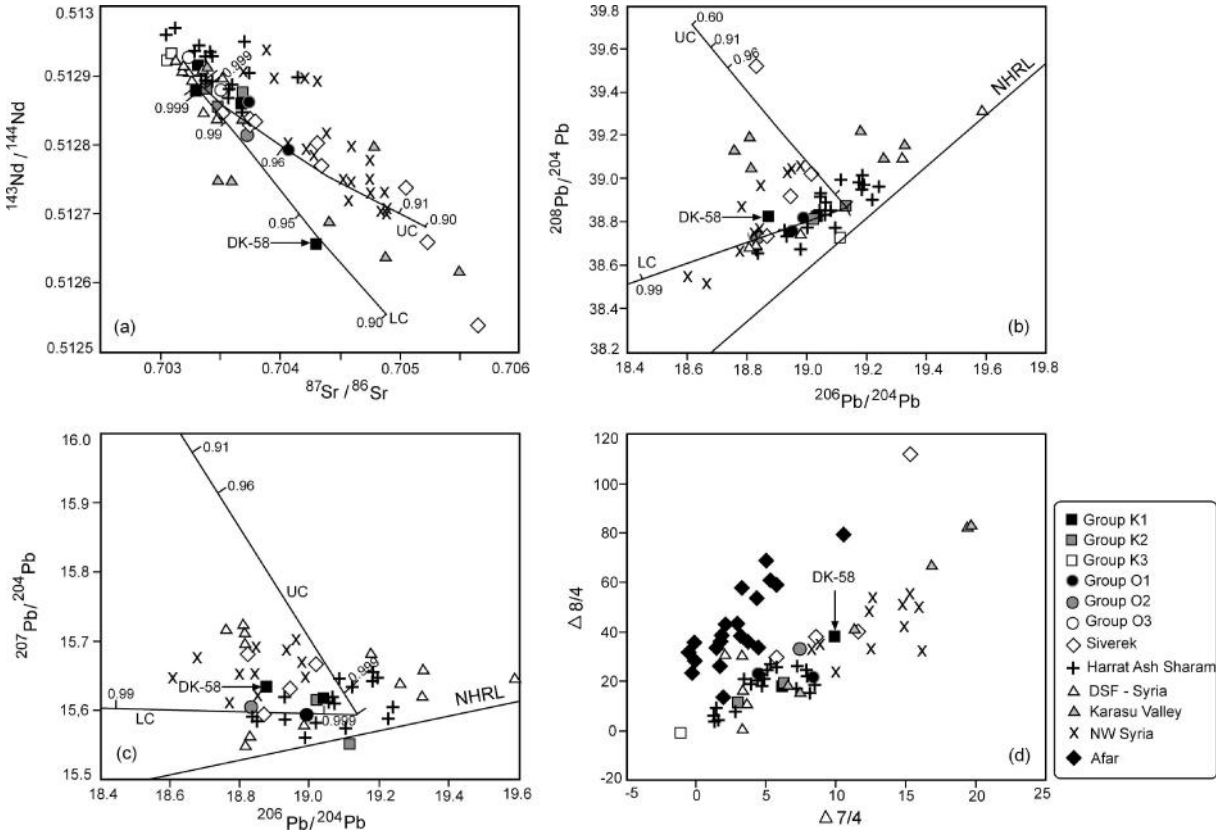
(a)
(b)
(c)
(d)
UC
LC
DK-58
NHRL
0.60
0.91
0.96
0.99
0.999
0.95
0.90
$^{143}Nd/^{144}Nd$
$^{87}Sr/^{86}Sr$
$^{208}Pb/^{204}Pb$
$^{206}Pb/^{204}Pb$
$^{207}Pb/^{204}Pb$
Δ8/4
Δ7/4
Group K1
Group K2
Group K3
Group O1
Group O2
Group O3
Siverek
Harrat Ash Sharam
DSF - Syria
Karasu Valley
NW Syria
Afar

Karacadağ 6

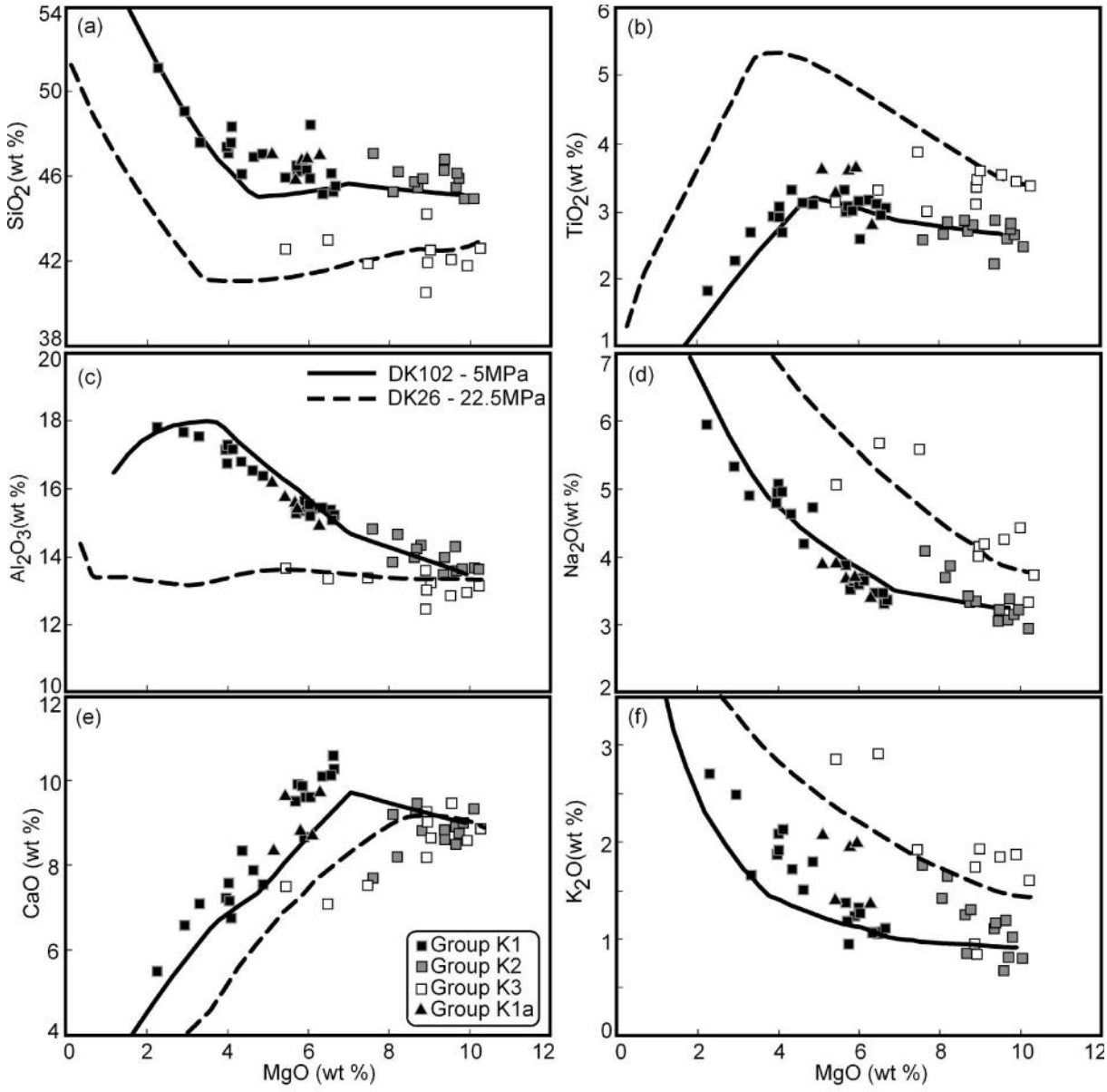
(a)
(b)
(c)
(d)
(e)
(f)
SiO2(wt %)
TiO2(wt %)
Al2O3(wt %)
Na2O(wt %)
CaO (wt %)
K2O(wt %)
MgO (wt %)
MgO (wt %)
DK102 - 5MPa
DK26 - 22.5MPa
Group K1
Group K2
Group K3
Group K1a

Karacadağ 7

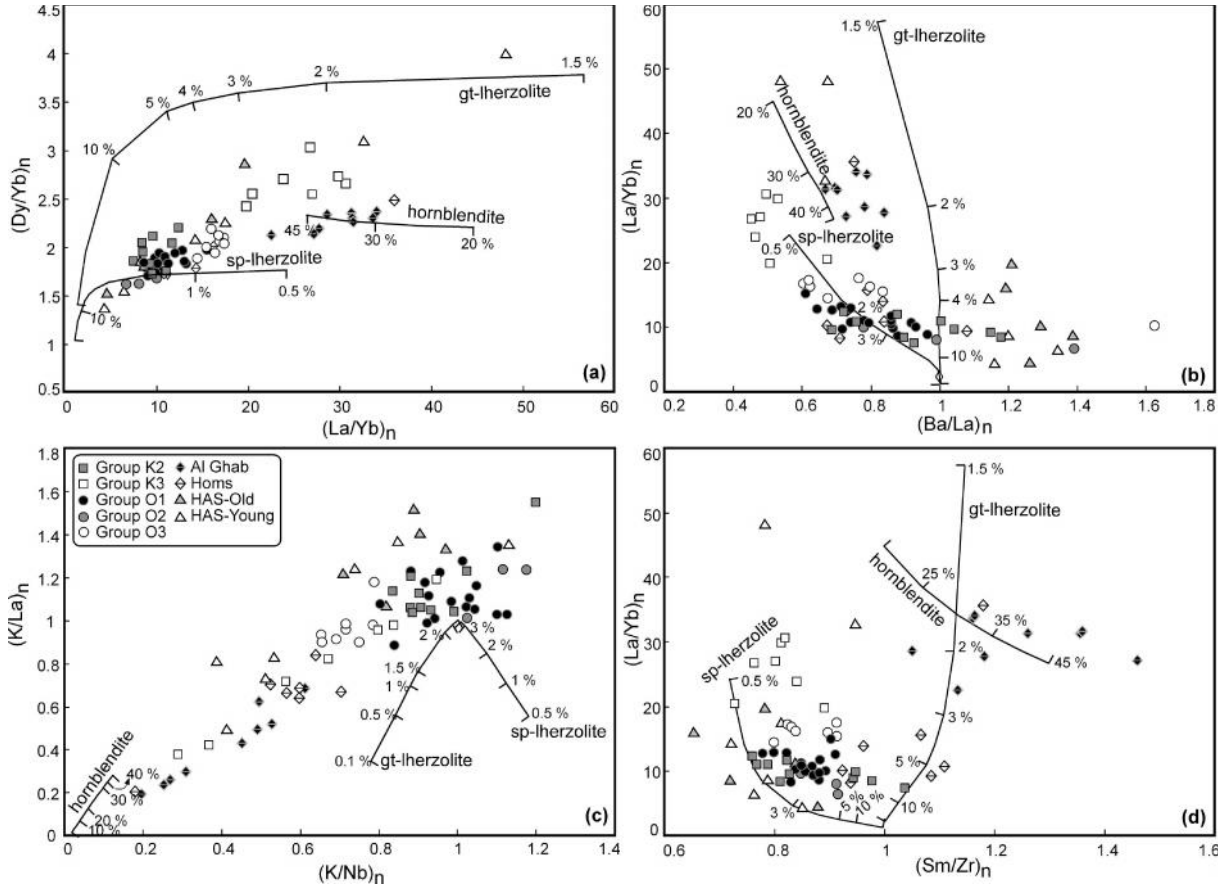
(a)
(Dy/Yb)n
(La/Yb)n
gt-lherzolite
hornblendite
sp-lherzolite
(b)
(La/Yb)n
(Ba/La)n
(c)
(K/La)n
(K/Nb)n
Group K2
Group K3
Group O1
Group O2
Group O3
Al Ghab
Homs
HAS-Old
HAS-Young
(d)
(Sm/Zr)n

Karacadağ 8

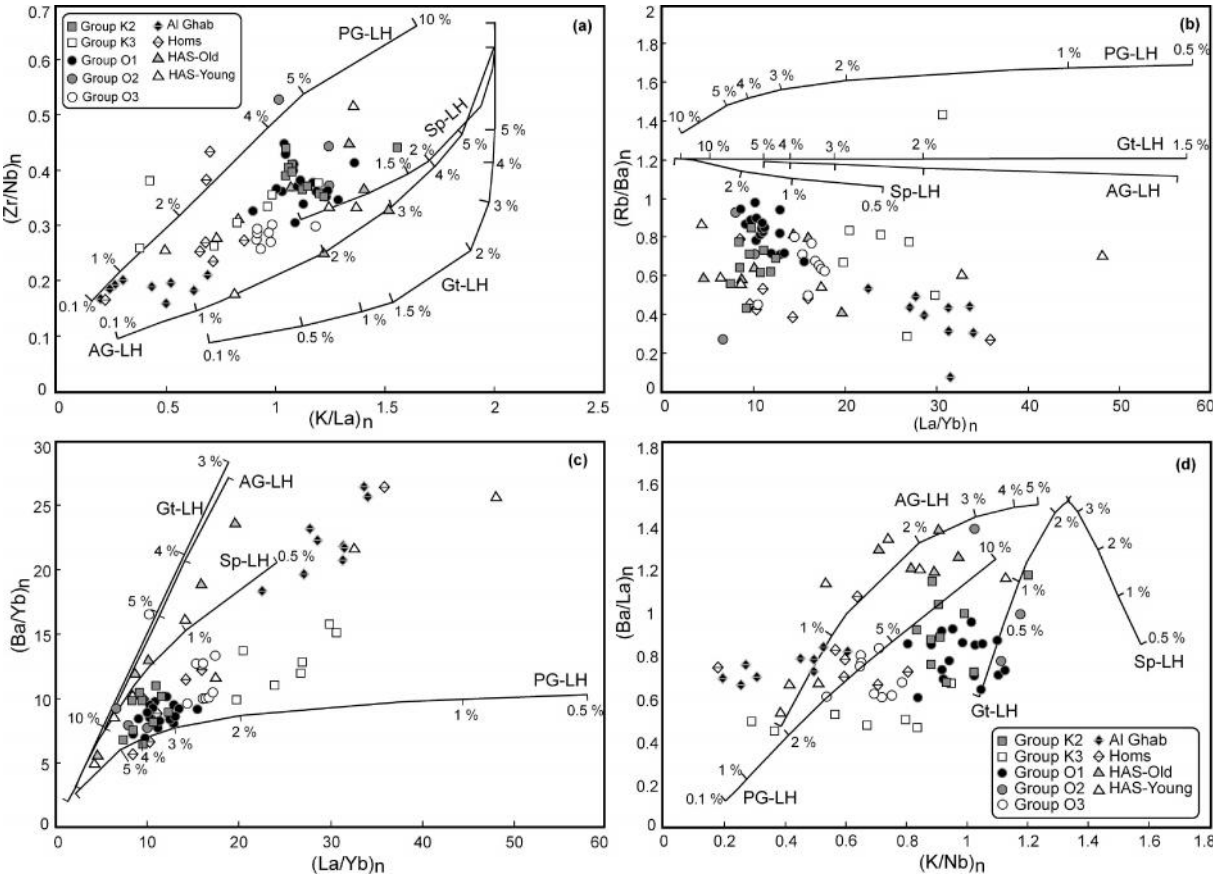
(a)
Group K2
Group K3
Group O1
Group O2
Group O3
Al Ghab
Homs
HAS-Old
HAS-Young
PG-LH
Sp-LH
Gt-LH
AG-LH
(Zr/Nb)n
(K/La)n
(b)
PG-LH
Gt-LH
Sp-LH
AG-LH
(Rb/Ba)n
(La/Yb)n
(c)
AG-LH
Gt-LH
Sp-LH
PG-LH
(Ba/Yb)n
(La/Yb)n
(d)
AG-LH
Sp-LH
Gt-LH
PG-LH
(Ba/La)n
(K/Nb)n

Karacadağ 9

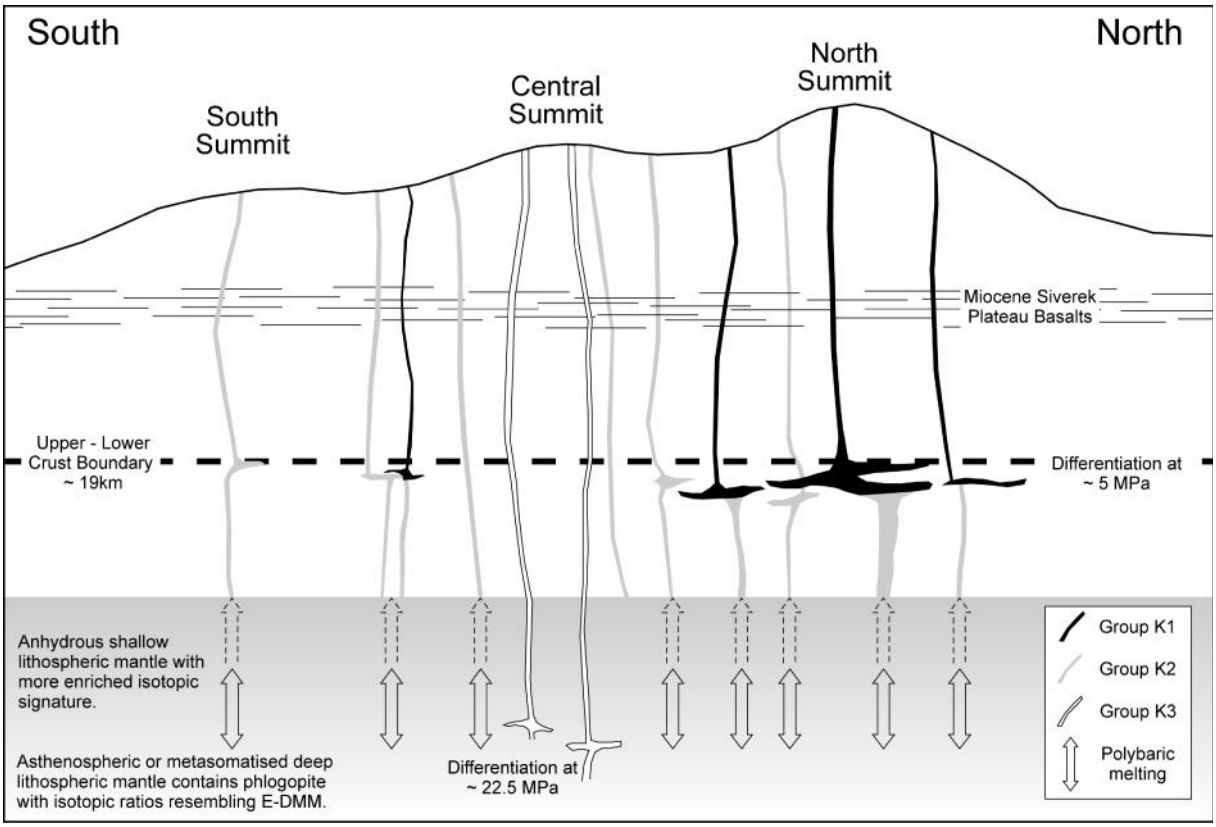

Karacadağ 10

1 Table 1: Major and trace element compositions of Karacadağ and Ovabağ lavas.

Sample	DK-1 (K1)	DK-2 (K1)	DK-3 (K1)	DK-4 (K1)	DK-5 (K1)	DK-6 (K1)	DK-7 (K1)	DK-8 (K1)
Latitude	37°42'35.64"N	37°42'22.44"N	37°42'55.98"N	37°42'47.34"N	37°42'49.38"N	37°42'43.32"N	37°42'15.72"N	37°42'5.22"N
Longitude	39°49'43.20"E	39°49'42.18"E	39°49'45.60"	39°49'37.26"E	39°49'28.68"E	39°50'6.30"E	39°50'23.52"E	39°50'27.12"E
SiO_2	46.15	46.12	45.92	45.91	46.33	45.48	46.93	48.34
TiO_2	3.04	3.29	3.10	3.25	3.10	3.03	3.10	2.67
Al_2O_3	15.38	16.82	15.44	15.60	15.40	15.19	16.55	17.22
Fe_2O_3	13.49	13.38	13.53	13.67	13.51	13.86	12.70	12.11
MgO	6.55	4.33	6.02	5.65	5.92	6.63	4.62	4.08
MnO	0.17	0.18	0.17	0.17	0.17	0.17	0.17	0.17
CaO	10.10	8.33	9.61	9.52	9.61	10.25	7.87	6.75
Na_2O	3.46	4.64	3.67	3.88	3.70	3.39	4.20	4.96
K_2O	1.06	1.71	1.29	1.37	1.24	1.09	1.51	2.13
P_2O_5	0.42	0.66	0.49	0.52	0.46	0.44	0.65	0.83
Cr_2O_3	0.019	0.001	0.001	0.007	0.013	0.020	0.014	0.007
LOI	-0.2	0.2	0.4	0.1	0.1	0.1	1.4	0.4
Total	99.65	99.66	99.66	99.66	99.66	99.67	99.71	99.67
Ni	72	20	55	54	67	69	31	28
Sc	24	13	21	20	22	24	14	11
V	293	229	290	297	292	313	229	139
Co	79.7	59.4	70.9	63.3	63.3	64.5	74.5	46.1
Cu	64.5	27.2	63.2	55.5	63.3	65.6	25.1	31.0
Zn	82	77	81	93	63	84	43	83
Ga	23.2	26.3	23.8	24.9	24.9	24.7	24.4	24.9
Rb	11.1	17.7	14.3	15.6	13.5	11.0	7.5	16.8
Sr	678	909	734	784	715	697	1009	1048
Y	21.1	24.6	22.9	22.6	22.0	22.9	23.6	23.8
Zr	173	243	198	202	189	177	253	323
Nb	28.4	48.9	34.5	37.7	33.3	29.9	37.8	48.5
Cs	0.3	0.4	0.3	0.4	0.4	0.2	0.3	0.2
Ba	179	273	201	220	220	170	197	237
La	21.1	33.2	25.4	27.0	24.1	22.0	30.4	39.7
Ce	47.7	71.1	55.7	58.3	53.2	49.0	67.6	85.0
Pr	6.11	8.86	7.08	7.36	6.70	6.33	8.53	10.33
Nd	26.1	36.6	29.3	31.3	28.5	26.6	34.7	41.0
Sm	5.76	7.66	6.32	6.56	6.24	6.14	7.13	7.86
Eu	2.14	2.67	2.28	2.33	2.22	2.24	2.65	2.85
Gd	5.95	7.19	6.54	6.56	6.09	6.32	6.87	7.31
Tb	0.92	1.07	0.95	0.99	0.95	0.96	1.01	1.04
Dy	4.49	5.29	4.80	4.75	4.66	4.69	5.03	5.15
Ho	0.84	0.94	0.88	0.88	0.82	0.88	0.91	0.89
Er	2.00	2.35	2.17	2.13	2.10	2.14	2.22	2.25
Tm	0.31	0.33	0.33	0.31	0.30	0.30	0.31	0.34
Yb	1.60	1.79	1.74	1.71	1.73	1.71	1.74	1.79
Lu	0.26	0.27	0.26	0.25	0.25	0.25	0.25	0.27
Hf	4.4	5.6	4.9	4.9	4.7	4.7	5.5	7.4
Ta	1.6	2.7	2.0	2.2	2.0	1.7	2.2	2.8
Pb	2.0	1.0	1.9	1.1	1.9	1.2	0.4	0.7
Th	2.1	3.1	2.5	2.7	2.5	2.1	2.9	3.4
U	0.7	1.1	0.9	0.9	0.7	0.7	1.0	1.3

2

3

4

Sample	DK-9 (K1)	DK-10 (K1)	DK-11 (K2)	DK-13 (K3)	DK-14 (K3)	DK-15 (K1a)	DK-16 (K1a)	DK-17 (K1a)
Latitude	37°41'48.60"N	37°41'46.80"N	37°41'46.08"N	37°41'24.90"N	37°41'19.02"N	37°40'54.30"N	37°40'51.24"N	37°41'1.74"N
Longitude	39°50'40.56"E	39°50'34.80"E	39°50'26.16"E	39°49'40.86"E	39°49'24.66"E	39°48'51.06"E	39°49'39.24"E	39°50'1.02"E
SiO_2	47.40	49.04	45.86	40.53	42.09	46.76	47.05	46.85
TiO_2	2.90	2.24	2.79	3.35	3.51	3.58	3.60	3.59
Al_2O_3	17.17	17.70	14.33	12.49	12.89	15.56	16.23	15.65
Fe_2O_3	12.41	11.12	12.93	14.16	14.31	12.54	12.33	12.66
MgO	3.95	2.92	8.81	8.90	9.53	5.81	5.10	5.88
MnO	0.17	0.18	0.16	0.18	0.18	0.15	0.15	0.15
CaO	7.20	6.57	8.79	9.28	9.46	8.83	8.36	8.65
Na_2O	4.80	5.33	3.33	4.02	4.26	3.64	3.90	3.59
K_2O	1.87	2.49	1.30	0.95	1.85	1.96	2.07	1.99
P_2O_5	0.72	0.87	0.47	1.06	1.03	0.50	0.52	0.51
Cr_2O_3	0.004	0.002	0.046	0.036	0.034	0.018	0.012	0.017
LOI	1.1	1.2	0.8	4.7	0.3	0.3	0.3	0.1
Total	99.68	99.63	99.63	99.63	99.49	99.65	99.65	99.65
Ni	20	20	132	184	181	70	51	61
Sc	7	7	21	17	18	19	17	19
V	166	152	260	278	277	305	295	310
Co	53.1	42.1	74.0	71.1	78.0	58.8	60.3	60.3
Cu	26.7	22.6	41.0	32.2	61.9	46.7	43.5	46.0
Zn	59	88	76	48	107	84	87	86
Ga	23.8	23.8	22.4	26.1	26.6	25.4	25.7	25.7
Rb	13.5	22.8	10.4	37.2	14.2	25.8	27.8	26.7
Sr	1038	1267	707	1262	1210	742	793	729
Y	24.8	26.2	20.6	22.0	23.1	23.1	23.8	22.9
Zr	278	421	193	314	319	224	235	224
Nb	43.4	60.9	33.6	74.8	74.8	39.6	42.4	40.2
Cs	0.2	0.2	0.2	0.2	0.3	0.5	0.6	0.6
Ba	216	250	186	285	311	285	306	306
La	34.2	50.1	24.1	56.6	57.8	28.4	30.0	28.4
Ce	65.6	102.8	52.1	111.7	115.9	61.5	64.5	62.5
Pr	9.37	12.19	6.42	13.42	13.70	7.86	8.08	7.72
Nd	38.5	47.6	26.2	54.1	53.3	32.4	34.0	32.8
Sm	7.83	8.82	5.71	9.93	10.01	6.82	7.15	7.02
Eu	2.79	2.92	2.06	3.33	3.46	2.32	2.38	2.34
Gd	7.29	7.69	5.63	8.86	8.99	6.53	6.78	6.65
Tb	1.09	1.10	0.86	1.15	1.24	0.99	1.02	1.02
Dy	5.53	5.31	4.25	5.13	5.51	4.76	4.95	5.04
Ho	0.91	0.99	0.76	0.83	0.86	0.85	0.86	0.88
Er	2.33	2.36	1.90	1.77	1.84	2.12	2.19	2.21
Tm	0.31	0.36	0.26	0.24	0.25	0.31	0.31	0.30
Yb	1.84	2.05	1.53	1.26	1.32	1.70	1.74	1.77
Lu	0.28	0.31	0.22	0.18	0.19	0.26	0.26	0.26
Hf	6.4	9.3	4.6	7.0	7.1	5.6	5.7	5.6
Ta	2.6	3.6	2.0	3.8	3.9	2.3	2.4	2.4
Pb	1.0	3.1	0.9	1.5	3.3	2.8	2.9	2.8
Th	2.5	5.1	2.2	5.5	5.2	3.5	4.1	3.7
U	1.1	1.4	0.7	2.0	1.9	1.1	1.2	1.1

5

6

7

Sample	DK-18 (K1)	DK-19 (K1)	DK-20 (K1)	DK-21 (K1)	DK-22 (K-3)	DK-23 (K-2)	DK-24 (K-3)	DK-25 (K-3)
Latitude	37°41'10.93"N	37°41'18.74"N	37°41'9.11"N	37°41'2.22"N	37°39'5.76"N	37°39'13.44"N	37°39'23.94"N	37°39'30.42"N
Longitude	39°49'47.22"E	39°49'57.09"E	39°50'16.70"E	39°50'25.62"E	39°50'12.30"E	39°49'39.48"E	39°49'39.84"E	39°49'40.56"E
SiO_2	47.61	51.11	47.03	47.46	41.80	45.44	41.90	42.60
TiO_2	2.65	1.79	3.07	3.02	3.43	2.61	3.85	3.13
Al_2O_3	17.56	17.82	16.40	17.29	13.01	14.27	13.42	13.71
Fe_2O_3	12.19	10.88	13.18	12.65	14.93	14.68	15.70	15.27
MgO	3.30	2.25	4.85	4.00	9.92	9.65	7.46	5.43
MnO	0.18	0.19	0.18	0.18	0.18	0.17	0.17	0.20
CaO	7.09	5.52	7.55	7.16	8.60	8.91	7.54	7.51
Na_2O	4.91	5.95	4.73	5.07	4.43	3.08	5.60	5.07
K_2O	1.66	2.70	1.80	1.92	1.87	0.67	1.92	2.86
P_2O_5	1.04	0.99	0.77	0.82	0.96	0.32	1.03	1.17
Cr_2O_3	0.002	0.002	0.010	0.002	0.027	0.038	0.015	0.010
LOI	1.5	0.5	0.1	0.1	0.3	-0.2	0.9	2.5
Total	99.68	99.69	99.68	99.67	99.49	99.66	99.51	99.45
Ni	20	20	41	20	206	223	119	76
Sc	9	9	14	10	17	21	10	8
V	112	44	185	129	247	246	258	155
Co	83.7	47.9	52.1	42.9	76.7	79.5	88.4	102.4
Cu	20.9	15.3	41.3	24.3	43.5	81.3	35.3	29.4
Zn	101	99	103	97	74	93	68	127
Ga	25.6	26.6	23.6	25.0	26.5	20.5	30.3	32.0
Rb	27.0	24.7	12.5	15.5	17.5	6.3	19.7	27.5
Sr	1132	991	896	960	1192	530	1214	1628
Y	26.3	26.7	23.7	25.9	22.1	16.9	19.9	25.2
Zr	318	375	267	294	315	109	430	501
Nb	59.2	62.2	36.3	54.2	63.6	18.3	73.6	102.5
Cs	0.4	0.3	0.2	0.2	0.2	0.1	0.3	0.4
Ba	283	343	178	231	248	124	274	409
La	46.0	51.9	33.1	38.3	51.0	13.2	55.2	74.8
Ce	97.0	107.3	72.9	83.2	104.4	30.2	115.7	155.8
Pr	12.10	12.84	9.14	10.45	12.75	4.00	13.89	18.88
Nd	47.3	49.8	37.2	42.0	51.8	17.7	55.8	74.0
Sm	8.99	8.93	7.47	8.28	9.76	4.37	10.65	13.50
Eu	1.24	2.97	2.54	2.86	3.32	1.62	3.46	4.38
Gd	8.04	7.77	6.67	7.54	8.58	4.46	9.03	11.26
Tb	1.17	1.12	0.98	1.12	1.17	0.70	1.13	1.44
Dy	5.52	5.29	4.82	5.33	5.03	3.44	4.86	5.80
Ho	0.97	0.98	0.87	0.98	0.82	0.64	0.75	0.95
Er	2.36	2.30	2.09	2.38	1.70	1.48	1.44	1.88
Tm	0.36	0.35	0.30	0.33	0.24	0.22	0.19	0.24
Yb	1.96	2.05	1.68	1.88	1.29	1.21	1.02	1.28
Lu	0.29	0.30	0.25	0.28	0.17	0.17	0.14	0.17
Hf	6.8	8.0	5.8	6.7	7.1	2.7	9.7	11.1
Ta	3.2	3.6	2.1	3.0	3.4	1.0	4.3	5.5
Pb	0.4	1.9	0.6	1.0	1.7	0.8	1.5	4.4
Th	3.5	4.5	2.2	3.1	4.7	1.1	5.1	6.6
U	1.3	1.7	1.0	1.2	1.8	0.4	2.1	2.3

8

9

10

Sample	DK-26 (K-3)	DK-27 (K-3)	DK-28 (K-3)	DK-29 (K-2)	DK-30 (K-2)	DK-31 (K1)	DK-32 (K1)	DK-52 (K-2)
Latitude	37°39'28.98"N	37°39'26.10"N	37°39'22.62"N	37°40'35.82"N	37°40'40.32"N	37°42'29.70"N	37°43'40.38"N	37°42'31.26"N
Longitude	39°50'9.78"E	39°50'6.66"E	39°50'3.00"E	39°50'52.02"E	39°50'42.84"E	39°50'11.28"E	39°49'51.96"E	39°38'59.04"E
SiO_2	42.60	43.02	42.54	47.07	46.26	45.37	45.20	44.90
TiO_2	3.35	3.28	3.55	2.58	2.84	2.97	3.10	2.48
Al_2O_3	13.30	13.39	13.30	14.83	14.65	15.11	15.44	13.64
Fe_2O_3	14.56	15.57	15.15	12.86	13.54	13.40	13.88	14.67
MgO	10.25	6.48	9.02	7.60	8.21	6.60	6.35	10.09
MnO	0.17	0.19	0.18	0.18	0.18	0.17	0.17	0.17
CaO	8.85	7.10	8.65	7.70	8.20	10.58	10.09	9.32
Na_2O	3.73	5.69	4.20	4.09	3.86	3.33	3.46	2.97
K_2O	1.60	2.92	1.93	1.76	1.65	1.09	1.06	0.80
P_2O_5	0.76	1.14	0.86	0.77	0.76	0.43	0.45	0.35
Cr_2O_3	0.037	0.010	0.027	0.036	0.041	0.021	0.012	0.040
LOI	0.3	0.7	0.1	0.1	0.1	0.6	0.0	0.2
Total	99.54	99.49	99.53	99.60	100.2	99.67	99.24	99.65
Ni	225	99	175	129	151	71	67	223
Sc	19	7	18	16	18	25	183	202
V	265	163	263	189	217	297	301	258
Co	87.7	60.2	77.6	62.2	67.8	65.4	71.4	80.1
Cu	62.1	25.0	57.1	47.9	56.5	62.3	63.1	67.8
Zn	103	100	119	85	92	83	93	92
Ga	24.8	31.0	27.0	24.1	23.2	23.0	24.1	20.3
Rb	11.7	28.1	15.5	14.7	14.0	11.5	9.8	8.0
Sr	1020	1511	1059	816	810	652	750	579
Y	20.7	22.8	21.8	23.2	22.0	21.6	21.8	17.2
Zr	248	482	303	282	260	173	176	130
Nb	45.8	92.3	52.6	42.6	41.1	27.8	29.7	20.6
Cs	0.2	0.4	0.2	0.1	0.2	0.2	0.1	0.1
Ba	192	358	209	266	228	173	183	202
La	37.4	67.8	44.1	37.2	34.2	20.4	21.2	17.3
Ce	81.0	141.4	95.5	75.0	72.3	46.1	48.3	38.6
Pr	10.00	17.39	11.91	9.34	8.80	6.01	6.44	4.96
Nd	40.7	68.9	48.8	36.2	36.0	25.3	26.7	20.9
Sm	8.53	12.90	9.84	7.11	7.09	5.95	6.14	4.74
Eu	2.78	4.13	3.27	2.43	2.33	1.99	2.26	1.71
Gd	7.53	10.76	8.44	6.52	6.30	5.67	6.14	4.76
Tb	1.04	1.35	1.15	0.93	0.94	0.91	1.05	0.75
Dy	4.78	5.76	5.21	4.39	4.18	4.37	4.83	3.61
Ho	0.79	0.86	0.82	0.82	0.83	0.80	0.99	0.68
Er	1.76	1.64	1.79	2.09	1.92	2.00	2.20	1.69
Tm	0.25	0.20	0.23	0.29	0.27	0.28	0.41	0.24
Yb	1.29	1.07	1.26	1.69	1.64	1.59	1.72	1.29
Lu	0.18	0.14	0.21	0.24	0.25	0.24	0.36	0.23
Hf	5.7	10.9	7.0	6.6	5.9	4.3	4.4	3.7
Ta	2.6	5.0	3.0	2.4	2.3	1.5	1.7	1.2
Pb	2.3	1.3	2.5	2.0	1.5	1.6	1.8	1.5
Th	2.9	5.7	3.3	3.4	2.7	2.2	2.1	1.9
U	1.1	2.3	1.4	1.2	1.1	0.7	0.6	0.6

11

12

13

Sample	DK-53 (K-2)	DK-55 (K-1)	DK-56 (K-2)	DK-57 (K-2)	DK-58 (K-1a)	DK-81 (K-3)	DK-83 (K-1)	DK-84 (K-2)
Latitude	37°45'14.46"N	37°51'24.90"N	37°54'40.50"N	37°54'40.20"N	37°53'10.32"N	37°39'5.46"N	37°38'10.08"N	37°37'6.72"N
Longitude	39°41'6.72"E	39°43'59.04"E	39°47'18.36"E	39°51'42.12"E	39°57'57.24"E	39°50'29.58"E	39°51'30.06"E	39°51'10.68"E
SiO_2	45.85	48.42	46.07	45.25	47.03	44.25	47.12	46.29
TiO_2	2.77	2.56	2.63	2.66	2.80	3.07	2.90	2.87
Al_2O_3	13.50	15.23	13.53	13.85	14.94	13.64	16.75	13.96
Fe_2O_3	14.99	13.17	14.33	13.81	12.60	14.22	12.50	13.93
MgO	9.73	6.03	9.67	8.09	6.28	8.92	4.00	9.39
MnO	0.17	0.16	0.16	0.17	0.15	0.17	0.18	0.17
CaO	8.78	8.70	8.48	9.19	9.71	8.20	7.58	8.62
Na_2O	3.11	3.64	3.38	3.70	3.44	4.17	4.95	3.06
K_2O	0.80	1.32	1.19	1.42	1.37	1.74	2.09	1.15
P_2O_5	0.38	0.52	0.43	0.59	0.39	0.71	1.09	0.34
Cr_2O_3	0.037	0.023	0.041	0.034	0.030	0.035	0.002	0.030
LOI	-0.5	-0.1	-0.3	0.9	1.0	0.4	0.5	-0.2
Total	99.65	99.68	99.65	99.67	99.72	99.56	99.63	99.64
Ni	224	51	208	182	106	193	20	207
Sc	153	253	261	219	260	224	284	20
V	254	246	244	244	258	231	139	285
Co	80.6	54.6	73.4	69.9	58.7	71.4	47.8	81.2
Cu	74.1	39.3	57.4	58.1	50.6	51.4	23.0	51.8
Zn	91	102	92	93	72	106	93	90
Ga	21.5	23.3	22.4	23.0	21.0	24.3	25.9	22.8
Rb	8.9	20.3	17.4	17.0	20.1	17.0	17.4	14.1
Sr	546	714	604	722	580	1039	1224	555
Y	18.6	23.9	20.5	22.1	20.4	19.0	25.3	20.2
Zr	133	188	196	235	177	256	324	157
Nb	20.1	25.4	27.4	31.4	22.9	41.9	55.6	21.9
Cs	0.3	0.3	0.5	0.4	0.5	0.2	0.2	0.2
Ba	153	253	261	219	260	224	284	199
La	16.9	30.1	25.7	32.7	21.5	32.7	46.9	16.6
Ce	39.1	64.7	54.4	70.4	47.0	68.5	95.8	36.2
Pr	5.05	8.25	6.76	8.87	6.00	8.60	11.89	5.02
Nd	21.4	33.5	29.0	36.1	25.5	34.0	48.2	21.3
Sm	5.02	7.09	5.97	6.90	5.43	7.20	8.73	4.92
Eu	1.87	2.31	2.01	2.33	1.85	2.50	2.98	1.77
Gd	5.25	6.89	5.78	6.70	5.43	6.28	7.45	4.75
Tb	0.78	0.99	0.85	0.95	0.81	0.91	1.09	0.75
Dy	4.06	4.91	4.28	4.67	4.23	4.26	5.35	4.23
Ho	0.72	0.89	0.78	0.83	0.73	0.65	0.90	0.71
Er	1.75	2.22	1.90	1.92	1.82	1.62	2.28	1.77
Tm	0.26	0.31	0.29	0.26	0.28	0.20	0.31	0.25
Yb	1.36	1.89	1.59	1.63	1.59	1.09	1.73	1.35
Lu	0.24	0.32	0.26	0.28	0.27	0.15	0.24	0.20
Hf	3.6	5.0	4.8	5.6	4.6	6.1	6.8	4.1
Ta	1.2	1.5	1.6	1.9	1.4	2.6	3.4	1.4
Pb	1.9	3.9	3.0	3.0	2.7	1.0	1.8	1.2
Th	2.2	3.6	3.0	3.8	2.5	2.9	4.1	1.9
U	0.5	8.0	1.0	1.2	0.8	1.1	1.5	0.7

14

15

16

Sample	DK-90 (K-2)	DK-93 (K-1)	DK-95 (K-2)	DK-97 (K-1)	DK-98 (K-1a)	DK-99 (K-3)	DK-102 (K-2)	DK-106 (K-2)
Latitude	37°35'32.28"N	37°33'45.60"N	37°33'44.16"N	37°32'4.80"N	37°32'25.92"N	37°38'13.32"N	37°42'24.60"N	37°36'53.76"N
Longitude	39°54'22.38"E	39°51'39.24"E	39°52'19.38"E	39°49'47.34"E	39°38'4.86"E	39°39'9.06"E	39°44'58.02"E	39°58'29.16"E
SiO_2	46.81	46.24	45.48	46.55	45.93	41.96	44.91	45.72
TiO_2	2.21	2.99	2.72	3.00	3.22	3.42	2.65	2.87
Al_2O_3	13.50	15.30	14.18	15.45	15.77	13.08	13.52	14.01
Fe_2O_3	13.27	13.93	14.79	14.08	13.27	15.29	14.55	13.57
MgO	9.37	5.71	8.68	5.75	5.42	8.94	9.84	8.64
MnO	0.17	0.17	0.18	0.17	0.16	0.18	0.19	0.17
CaO	8.82	9.92	9.45	9.88	9.64	9.03	9.00	9.25
Na_2O	3.24	3.70	3.34	3.53	3.88	4.17	3.19	3.42
K_2O	1.11	1.18	0.85	0.94	1.40	0.84	1.02	1.25
P_2O_5	0.43	0.57	0.41	0.43	0.56	0.98	0.46	0.56
Cr_2O_3	0.043	0.018	0.039	0.011	0.011	0.030	0.041	0.047
LOI	0.7	-0.1	0.5	-0.1	0.4	1.6	0.2	0.1
Total	99.64	99.67	99.66	99.70	99.66	99.53	99.61	99.64
Ni	205	78	165	51	53	191	227	145
Sc	19	21	21	21	18	16	20	19
V	222	281	284	302	280	279	273	267
Co	69.7	62.1	71.7	63.0	55.5	69.3	79.9	64.3
Cu	38.2	56.7	74.2	49.7	64.5	44.8	59.7	42.6
Zn	92	81	94	79	71	99	77	82
Ga	21.4	24.0	21.3	22.5	23.9	25.9	21.1	21.3
Rb	15.1	12.3	9.8	7.0	14.4	5.4	10.8	10.6
Sr	597	758	599	683	883	1302	737	741
Y	21.1	23.1	19.3	20.0	22.7	21.5	19.6	20.5
Zr	166	183	136	163	194	324	171	201
Nb	28.0	31.2	20.8	22.8	31.3	52.5	26.4	27.9
Cs	0.2	0.2	0.2	0.1	0.3	0.2	0.2	0.1
Ba	234	185	127	125	252	205	191	168
La	22.1	24.7	18.2	17.8	23.0	44.7	21.6	22.8
Ce	46.4	51.8	37.5	37.7	48.9	91.9	45.6	50.3
Pr	6.02	6.76	5.17	5.15	6.72	12.10	6.05	6.65
Nd	25.3	30.1	22.1	22.8	28.7	47.7	26.1	28.2
Sm	5.30	6.16	4.97	5.06	6.16	9.55	5.44	5.90
Eu	1.85	2.18	1.84	1.93	2.16	3.18	1.95	2.05
Gd	5.05	5.72	4.78	4.96	5.83	7.99	5.00	5.31
Tb	0.81	0.90	0.75	0.79	0.90	1.11	0.80	0.83
Dy	4.21	4.90	4.20	4.07	4.57	5.28	3.95	4.24
Ho	0.72	0.83	0.67	0.73	0.75	0.77	0.68	0.75
Er	1.96	2.05	1.76	1.77	1.94	1.81	1.68	1.88
Tm	0.27	0.29	0.24	0.24	0.28	0.22	0.23	0.27
Yb	1.59	1.60	1.30	1.37	1.48	1.14	1.26	1.26
Lu	0.22	0.23	0.19	0.20	0.23	0.17	0.19	0.21
Hf	4.5	4.8	4.0	3.9	4.6	7.9	4.1	5.0
Ta	1.7	1.7	1.2	1.3	2.0	3.1	1.6	1.8
Pb	0.6	1.5	0.9	1.0	1.5	2.4	1.5	1.0
Th	2.8	2.6	1.9	1.8	1.8	4.7	3.9	1.7
U	0.8	0.7	0.6	0.6	0.6	1.4	0.7	0.8

17

18

19

Sample	DO-59 (O-1)	DO-60 (O-1)	DO-61 (O-1)	DO-62 (O-2)	DO-63 (O-1)	DO-64 (O-3)	DO-65 (O-3)
Latitude	37°41'24.84"N	37°41'24.72"N	37°42'28.50"N	37°41'5.04"N	37°41'42.24"N	37°39'11.34"N	37°39'8.35"N
Longitude	40° 1'10.20"E	40° 1'13.14"E	40° 3'25.68"E	40° 3'46.80"E	40° 4'7.08"E	40° 0'4.38"E	40° 0'13.52"E
SiO_2	47.29	47.21	44.82	46.50	47.41	44.18	43.64
TiO_2	2.31	2.42	2.84	2.67	2.47	3.32	3.22
Al_2O_3	13.22	13.38	13.54	14.53	13.61	13.43	13.10
Fe_2O_3	12.78	13.17	14.23	13.66	13.17	14.91	14.42
MgO	10.44	10.37	9.11	8.22	9.88	9.95	9.75
MnO	0.16	0.16	0.17	0.17	0.16	0.18	0.17
CaO	8.55	8.25	9.00	8.98	8.35	9.10	8.83
Na_2O	3.06	3.09	3.44	3.45	3.06	4.03	4.08
K_2O	1.21	1.26	1.51	1.51	1.27	1.80	1.69
P_2O_5	0.43	0.44	0.67	0.47	0.46	0.70	0.71
Cr_2O_3	0.049	0.047	0.035	0.038	0.044	0.032	0.032
LOI	0.1	-0.2	0.2	-0.2	-0.3	0.0	-0.1
Total	99.64	99.64	99.60	99.65	99.63	101.65	99.56
Ni	242	245	178	110	231	181	174
Sc	21	21	21	21	21	19	19
V	229	233	253	260	237	267	255
Co	70.4	72.1	70.4	64.6	72.9	82.5	72.2
Cu	41.9	54.9	60.1	46.3	54.5	52.1	49.2
Zn	65	86	106	91	85	94	69
Ga	20.6	21.4	22.7	22.4	22.1	24.9	25.0
Rb	18.1	17.4	14.5	14.0	17.7	15.7	15.3
Sr	568	602	894	678	610	949	934
Y	20.0	21.5	24.0	24.4	21.8	24.7	24.4
Zr	162	173	219	187	178	267	255
Nb	26.3	27.9	41.1	30.9	29.4	57.2	55.5
Cs	0.8	0.7	0.2	0.3	0.8	0.2	0.2
Ba	202	221	234	216	228	258	261
La	23.1	25.4	37.8	27.3	25.9	41.8	41.3
Ce	48.3	52.3	76.5	56.5	53.0	86.0	83.9
Pr	6.14	6.55	9.61	7.32	6.84	10.87	10.71
Nd	25.2	27.8	40.0	31.6	28.2	44.7	44.4
Sm	5.33	5.65	7.64	6.13	5.78	8.56	8.31
Eu	1.90	1.93	2.59	2.27	1.98	2.86	2.74
Gd	5.35	5.74	7.44	6.31	5.83	8.13	7.82
Tb	0.82	0.86	1.09	0.94	0.88	1.14	1.01
Dy	4.18	4.42	5.10	4.91	4.60	5.42	5.27
Ho	0.76	0.81	0.90	0.90	0.83	0.93	0.89
Er	1.83	1.91	2.16	2.18	1.98	2.10	2.05
Tm	0.27	0.30	0.29	0.33	0.31	0.31	0.30
Yb	1.55	1.59	1.67	1.87	1.66	1.70	1.64
Lu	0.25	0.28	0.28	0.30	0.28	0.27	0.26
Hf	4.1	4.3	5.6	4.8	4.5	6.7	6.3
Ta	1.6	1.7	2.5	1.9	1.8	3.4	3.2
Pb	2.1	3.3	2.7	2.7	2.8	2.6	2.3
Th	3.0	3.2	3.4	3.0	2.9	3.6	3.6
U	1.1	0.9	1.0	0.9	0.8	1.3	1.3

20

21

22

Sample	DO-66 (O-3)	DO-67 (O-3)	DO-68 (O-1)	DO-69 (O-1)	DO-70 (O-1)	DO-71 (O-1)	DO-72 (O-1)
Latitude	37°39'7.20"N	37°39'7.62"N	37°42'28.62"N	37°40'13.44"N	37°39'10.86"N	37°38'13.32"N	37°36'56.58"N
Longitude	40° 0'29.10"E	40° 0'29.34"E	40° 8'10.98"E	39°59'10.38"E	39°58'49.08"E	39°58'14.22"E	39°58'44.58"E
SiO_2	44.48	44.95	46.28	47.06	46.92	47.26	47.18
TiO_2	2.88	2.73	2.76	2.78	2.68	2.52	2.44
Al_2O_3	13.14	13.22	13.97	14.24	13.26	13.23	13.37
Fe_2O_3	14.76	14.29	13.55	13.89	14.28	13.36	13.65
MgO	9.52	9.66	9.44	9.73	9.57	10.06	10.01
MnO	0.17	0.17	0.16	0.17	0.16	0.16	0.16
CaO	8.57	8.61	8.25	8.35	8.09	8.34	8.24
Na_2O	3.94	3.77	3.37	3.46	3.34	3.27	3.17
K_2O	1.74	1.62	1.33	1.38	1.36	1.20	1.19
P_2O_5	0.71	0.61	0.53	0.56	0.48	0.43	0.44
Cr_2O_3	0.032	0.035	0.046	0.047	0.035	0.045	0.043
LOI	-0.4	-0.1	-0.1	0.0	-0.6	-0.3	-0.3
Total	99.57	99.60	99.62	101.69	99.61	99.62	99.62
Ni	176	191	194	213	227	235	234
Sc	19	20	19	20	19	20	20
V	240	235	242	247	229	233	218
Co	74.5	74.3	69.8	73.5	77.5	73.1	75.5
Cu	45.1	49.1	53.9	52.1	65.5	58.9	57.6
Zn	99	65	88	92	95	92	89
Ga	24.5	22.8	21.2	22.3	23.7	21.4	21.7
Rb	19.1	18.7	13.8	14.7	16.1	16.6	15.4
Sr	878	814	705	762	663	625	613
Y	24.7	24.4	20.5	21.6	22.0	22.1	22.4
Zr	240	235	242	203	197	172	175
Nb	52.8	47.0	27.5	27.9	29.7	29.1	29.5
Cs	0.4	0.4	0.2	0.2	0.5	0.5	0.5
Ba	272	254	209	224	187	209	201
La	43.2	37.0	28.6	29.8	28.6	26.3	26.7
Ce	85.1	72.9	58.4	59.9	56.4	52.0	52.1
Pr	10.67	9.39	7.4	7.65	7.37	6.90	6.69
Nd	42.7	37.4	31.8	32.1	31.1	28.6	28.6
Sm	8.01	7.08	5.92	6.11	6.26	5.75	5.68
Eu	2.73	2.41	2.15	2.18	2.15	2.02	2.03
Gd	7.81	7.09	5.88	5.91	6.18	5.73	5.90
Tb	1.11	1.03	0.85	0.85	0.93	0.88	0.89
Dy	5.41	5.07	4.20	4.50	4.57	4.50	4.60
Ho	0.94	0.90	0.75	0.80	0.84	0.79	0.83
Er	2.15	2.15	1.83	1.92	1.98	1.93	1.91
Tm	0.32	0.32	0.28	0.28	0.28	0.29	0.30
Yb	1.81	1.75	1.48	1.57	1.51	1.64	1.67
Lu	0.29	0.28	0.24	0.30	0.25	0.26	0.26
Hf	6.2	5.7	5.1	4.9	5.3	4.6	4.4
Ta	3.1	2.7	1.7	1.8	1.9	1.8	1.8
Pb	2.1	2.1	1.0	1.0	3.0	2.4	2.6
Th	4.5	3.7	2.3	2.7	3.3	2.9	3.0
U	1.4	1.2	0.8	0.9	1.1	0.9	0.9

23

24

25

26

Sample	DO-73 (O-1)	DO-74 (O-1)	DO-75 (O-1)	DO-76 (O-1)	DO-77 (O-3)	DO-78 (O-3)	DO-107 (O-1)
Latitude	37°36'33.96"N	37°35'56.46"N	37°35'45.84"N	37°35'51.18"N	37°37'10.86"N	37°37'47.04"N	37°37'1.62"N
Longitude	39°59'11.46"E	39°59'40.14"E	40° 1'12.00"E	40° 3'33.96"E	40° 4'45.36"E	40°10'58.26"E	39°58'37.74"E
SiO_2	47.05	47.80	45.68	47.31	44.05	45.88	46.73
TiO_2	2.35	2.40	2.62	2.53	3.31	2.43	2.50
Al_2O_3	13.39	13.50	13.35	13.25	12.58	12.79	13.62
Fe_2O_3	14.12	13.36	13.63	13.25	14.74	13.63	13.22
MgO	10.27	10.17	10.29	10.01	10.59	11.25	10.35
MnO	0.16	0.16	0.17	0.16	0.18	0.17	0.17
CaO	8.71	8.07	8.69	8.36	9.47	8.73	8.56
Na_2O	3.16	3.27	3.34	3.36	3.55	3.16	3.12
K_2O	1.08	1.13	1.30	1.22	1.45	1.20	1.23
P_2O_5	0.40	0.39	0.53	0.47	0.70	0.46	0.44
Cr_2O_3	0.041	0.045	0.042	0.044	0.038	0.043	0.046
LOI	-0.6	-0.7	-0.1	-0.4	0.0	-0.2	-0.4
Total	99.64	99.64	99.58	99.61	100.69	99.58	99.64
Ni	241	255	213	234	227	251	246
Sc	21	21	21	20	21	21	21
V	215	213	225	215	267	221	221
Co	73.9	68.8	76.9	70.1	74.2	71.3	78.4
Cu	61.5	59.2	46.0	60.0	56.3	57.7	50.2
Zn	89	87	101	87	105	91	80
Ga	20.8	21.9	21.0	22.1	23.3	20.7	21.0
Rb	13.4	14.5	15.4	16.2	12.8	15.3	15.3
Sr	546	503	752	582	886	637	583
Y	20.9	20.3	21.7	21.8	23.9	20.8	20.0
Zr	158	158	184	183	228	168	173
Nb	24.1	23.4	36.8	31.6	50.8	34.7	29.4
Cs	0.2	0.3	0.3	0.5	0.2	0.2	0.5
Ba	164	167	235	197	291	377	212
La	22.5	18.7	26.8	22.3	35.8	22.8	22.4
Ce	45.3	41.5	59.3	51.0	77.2	51.0	47.1
Pr	6.02	5.37	7.44	6.43	9.67	6.50	6.44
Nd	25.2	22.1	30.5	27.7	38.6	27.2	27.7
Sm	5.33	5.06	6.27	5.92	7.90	5.50	5.96
Eu	1.86	1.82	2.09	1.95	2.67	1.94	1.90
Gd	5.35	5.38	6.09	5.98	7.65	5.51	5.56
Tb	0.86	0.85	0.90	0.89	1.07	0.83	0.84
Dy	4.56	4.23	4.60	4.44	5.13	4.30	4.21
Ho	0.80	0.75	0.80	0.82	0.87	0.77	0.78
Er	1.88	1.78	2.04	1.94	2.09	1.89	1.99
Tm	0.28	0.26	0.27	0.27	0.29	0.28	0.24
Yb	1.58	1.49	1.53	1.49	0.22	1.52	1.49
Lu	0.26	0.22	0.23	0.22	0.22	0.24	0.21
Hf	4.2	4.1	4.6	4.7	5.7	4.3	4.7
Ta	1.4	1.4	2.2	2.0	3.0	2.0	1.9
Pb	2.4	2.5	2.5	3.8	2.0	2.3	2.1
Th	2.5	2.2	3.4	3.4	3.6	3.3	2.7
U	0.7	0.4	1.0	0.9	1.1	0.8	0.7

27

28

Sample	DO-108 (O-1)	DO-109 (O-1)	DO-110 (O-2)	DO-113 (O-2)	DO-114 (O-3)	DO-117 (O-3)	DO-120 (O1)
Latitude	37°38'19.56"N	37°43'0.90"N	37°43'27.18"N	37°41'6.34"N	37°40'17.88"N	37°37'32.52"N	37°38'4.98"N
Longitude	39°58'16.20"E	40° 0'6.54"E	40°15'38.34"E	40°10'23.70"E	40°13'52.50"E	40° 9'36.66"E	40° 6'7.80"E
SiO_2	47.03	45.14	47.60	48.37	45.07	42.12	47.50
TiO_2	2.47	2.80	2.04	2.26	2.76	3.27	2.25
Al_2O_3	13.39	13.50	14.35	13.87	13.12	12.20	13.41
Fe_2O_3	13.38	13.52	13.74	13.45	13.65	14.96	13.64
MgO	10.10	9.13	9.12	8.81	10.42	10.50	9.72
MnO	0.17	0.17	0.17	0.17	0.18	0.19	0.17
CaO	8.32	9.06	8.52	8.33	9.15	9.91	8.25
Na_2O	3.20	3.53	2.88	3.26	3.15	3.44	3.24
K_2O	1.23	1.48	0.72	1.12	1.50	1.60	1.29
P_2O_5	0.45	0.59	0.28	0.36	0.62	0.81	0.41
Cr_2O_3	0.046	0.038	0.046	0.044	0.038	0.039	0.040
LOI	-0.2	0.7	0.2	-0.4	-0.1	0.5	-0.3
Total	99.63	99.65	99.67	99.67	99.59	99.53	99.64
Ni	241	185	185	165	221	220	207
Sc	21	21	23	23	22	21	21
V	238	247	229	227	260	279	213
Co	77.2	70.9	76.8	66.7	88.9	86.9	68.7
Cu	49.9	48.0	37.3	40.2	44.3	51.0	43.0
Zn	81	94	77	79	75	90	88
Ga	22.0	23.8	21.1	20.9	22.3	23.0	19.2
Rb	16.5	15.6	5.6	17.3	19.1	17.4	17.5
Sr	604	766	401	487	859	961	537
Y	20.9	22.2	20.7	20.9	23.2	23.7	21.3
Zr	180	202	137	156	211	235	164
Nb	30.6	36.4	16.0	21.7	48.1	56.0	29.0
Cs	0.5	0.2	0.1	0.2	0.2	0.2	0.4
Ba	217	207	225	205	294	301	220
La	23.2	29.5	15.9	20.3	34.6	38.7	22.5
Ce	48.5	62.1	34.8	43.6	70.0	79.7	46.7
Pr	6.56	8.24	4.74	5.87	9.00	10.38	6.07
Nd	28.8	34.5	21.8	26.0	37.0	45.0	27.1
Sm	6.02	7.10	4.85	5.50	7.44	8.29	5.57
Eu	1.87	2.25	1.55	1.68	2.23	2.64	1.74
Gd	5.58	6.35	4.66	5.04	6.56	7.31	5.30
Tb	0.89	0.99	0.77	0.83	0.95	1.08	0.83
Dy	4.24	4.85	4.04	4.29	4.69	5.03	4.51
Ho	0.81	0.84	0.78	0.84	0.84	0.85	0.85
Er	2.13	2.11	2.19	2.13	2.29	2.03	2.02
Tm	0.27	0.29	0.29	0.29	0.30	0.28	0.28
Yb	1.47	1.58	1.63	1.72	1.54	1.51	1.70
Lu	0.21	0.21	0.26	0.26	0.24	0.23	0.25
Hf	4.3	5.6	4.0	4.7	5.3	6.1	4.4
Ta	2.0	2.2	1.1	1.4	2.9	3.3	1.8
Pb	1.6	1.2	1.9	1.5	2.2	2.2	2.2
Th	2.4	2.4	3.0	4.2	4.4	5.5	2.9
U	0.9	1.0	0.3	0.6	1.2	1.4	0.8

29

Table 2: Karacadağ and Ovabağ Isotopic Results

Sample	$^{143}Nd/^{144}Nd$	$^{87}Sr/^{86}Sr$	$^{206}Pb/^{204}Pb$	$^{207}Pb/^{204}Pb$	$^{208}Pb/^{204}Pb$
DK-1 (K-1)	0.512863	0.703687	19.032	15.616	38.823
DK-10 (K-1)	0.512916	0.703321			
DK-19 (K-1)	0.512880	0.703303			
DK-23 (K-2)	0.512856	0.703484	19.018	15.615	38.816
DK-25 (K-3)	0.512924	0.703065	19.113	15.552	38.728
DK-27 (K-3)	0.512933	0.703095			
DK-29 (K-2)	0.512881	0.703379	19.130	15.595	38.874
DK-52 (K-2)	0.512878	0.703683			
DK-58 (K-1a)	0.512657	0.704303	18.873	15.636	38.828
DO-59 (O-1)	0.512794	0.704063	18.948	15.628	38.752
DO-62 (O-2)	0.512816	0.703722	18.832	15.606	38.729
DO-64 (O-3)	0.512928	0.703235			
DO-67 (O-3)	0.512880	0.703501			
DO-68 (O-1)	0.512864	0.703726	18.989	15.594	38.820